THESIS

CORROSION TESTING OF ALLOYS FOR BIOMASS COOKSTOVE COMBUSTORS

Submitted by

Kelly Banta

Department of Mechanical Engineering

In partial fulfillment of the requirements

For the Degree of Master of Science

Colorado State University

Fort Collins, Colorado

Spring 2017

Master's Committee:

Advisor: Anthony Marchese

John Mizia
Shantanu Jathar
Justin Sambur

ABSTRACT

CORROSION TESTING OF ALLOYS FOR BIOMASS COOKSTOVE COMBUSTORS

Worldwide, over 3 billion people use biomass for cooking and heating. Many people cook over 3-stone fires or inefficient and highly polluting traditional cookstoves, presenting a large human health risk and significant climate impacts. One solution to this is the development of improved cookstoves, which can alleviate this burden by being more efficient and cleaner-burning.

To be effective in their purpose, improved cookstoves must be long-lasting. Achieving longevity is challenging from a material corrosion perspective, particularly in the case of metallic combustors, because cookstove combustors must operate at high temperatures (> 600^{o}C) in environments with corrosive species released from biomass combustion. A key part of this challenge is cost, since materials must be inexpensive to permit widespread adoption in the developing world; however, corrosion resistant materials are typically costlier.

In this work, screening protocols for corrosion testing of cookstove combustor materials were developed and shown to be effective methods for accelerated corrosion testing, and a number of alloys were evaluated for corrosion performance. Additionally, a FeCrSi alloy was identified as a potentially low-cost material with high corrosion resistance in cookstove applications. This alloy is currently being patented.

TABLE OF CONTENTS

LIST OF TABLES

LIST OF FIGURES

CHAPTER 1: INTRODUCTION

1.1 Background

Around 3 billion people worldwide use biomass for cooking and heating [1], [2]. Traditional cooking methods are frequently inefficient and release large quantities of harmful pollution as a result. Poor household air quality leads to over 4 million premature deaths annually from illnesses such as pneumonia, stroke, ischemic heart disease, chronic obstructive pulmonary disease, and lung cancer [2], [3]. Emissions from biomass combustion also have climate forcing impacts [4]–[6]. Recently, efforts to develop and promote adoption of improved cookstoves with increased efficiency and reduced emissions have been increasing [7]. Goals are to improve health and climate effects and risks to personal safety, as well as to enable reduced consumption of fuel, meaning less time and money spent gathering or purchasing fuel for families, and lower deforestation in areas where forest resources may be diminishing [2], [5], [8].

In order to be truly effective in realizing the goals of reduced fuel use and lower pollution, well-performing stoves must also be user-friendly and compatible with respect to cooking practices [9], as well as long-lasting and durable. One of the important considerations for durability is the choice of construction materials. A number of materials are used in both traditional and improved cookstoves; metal, ceramic, mud or sand-clay mixtures, and concrete are common building materials [10]. While ceramic or mud chambers can be cheaper than metallic chambers [7], many improved cookstove designs use metallic chambers. Metallic chambers can provide many benefits over other materials such as greater consistency in manufacturing, improved

performance, lower mass, more robustness, and greater design flexibility [10]. However, metallic stove parts are more susceptible to corrosion than ceramic parts.

Corrosion represents a large challenge for metallic combustors, since they must operate at high temperatures (> 600^{o}C) in environments with corrosive species released from biomass combustion. A key part of this challenge is cost, since materials must be inexpensive in order to permit widespread adoption in the developing world; however, metals with higher corrosion resistance tend to be more expensive, due to the high cost of alloying elements such as nickel.

An example of how severe corrosion in a cookstove can be is shown in **Figure 1**.

Figure 1: *Charcoal stove fuel grates, new (left) and corroded (right).*

Corrosion in this high temperature context involves the formation of a layer of oxide scale on the surface of the metal. If the oxide layer is solid and continuous, it can serve as a protective layer against further corrosion, providing a barrier between the hot gaseous environment above and the base metal below [11]. In this case, the limiting factor of the corrosion rate is the diffusion rate of species through the oxide layer, and the corrosion rate decreases with time. On the other hand, a porous oxide layer allows species to come directly in contact with the base metal, reducing or

eliminating the oxide layer's protectiveness, and resulting in a corrosion rate that is linear with time [12]. While corrosion cannot be prevented entirely, it is desirable for the oxide layer to be continuous and well-adhered to the base metal, and for the base metal to show minimal internal attack.

In research of high temperature corrosion, the effects on steel of a large range of alloying elements, including Ni, Mo, Mn, Ti, N, Al, Cr, and Si, have been studied [13]. In particular, additions of aluminum and/or silicon into iron-chromium alloys have been shown to increase high temperature corrosion resistance [14]–[17]. The source of this increased corrosion resistance in these alloys is the formation of protective oxide layers based on Al_2O_3, Cr_2O_3, and/or SiO_2 [11]. Moreover, Al and Si are inexpensive compared to other elements such as Ni, an alloying element used in many stainless steels and also a large driver of cost [18].

Corrosion in the context of biomass combustion has been studied, particularly with respect to biomass fired power generation applications [19]–[22]. Conditions encountered in biomass-fired boilers are similar to those of biomass cookstoves in that the materials are exposed to a similar high temperature environment in the presence of corrosive species. However, biomass cookstoves present different conditions with respect to temperatures, pressures, fuels, and species present.

1.2 Testing overview

The work discussed in this manuscript was completed for a grant awarded by the U.S. Department of Energy. The grant was awarded to Oak Ridge National Lab (ORNL) to complete

the project, and the in-situ portion of the testing was carried out as a collaboration between ORNL and the Advanced Biomass Combustion Laboratory at Colorado State University (CSU). Brief description will be given to the work completed at ORNL; however, this document will focus on the portion of the work completed at Colorado State University. More details regarding the portion of the work completed at ORNL can be found in the publication resulting from this work, entitled "Alloy Corrosion Considerations in Low-Cost, Clean Biomass Cookstoves for the Developing World", published in the April 2017 issue of Energy for Sustainable Development [23].

The goals of this project were to 1) develop testing protocols for the evaluation of the corrosion performance of cookstove combustor materials 2) to test an array of potential cookstove combustor materials, both commercial and developmental, in order to achieve insight into the corrosion behavior of stainless steels and other alloys in the context of biomass cookstoves, and 3) to identify approaches for low-cost alloy and coating design.

Two methods were used for testing the materials: 1) In-situ testing and 2) lab furnace testing. Lab furnace testing was completed at ORNL and in-situ cookstove testing was completed at CSU. Testing setups are shown in **Figure 2**.

a) b)

Figure 2: *Photographs of coupons in (a) lab furnace test and (b) in-situ cookstove test.*

Both tests were carried out to a total of 1000 hours of exposure, representing a year of use if a stove is used for ~2.7 hours per day. However, it should be noted that the use of salt species accelerated the corrosion in this testing.

1.2.1 In-situ testing

Envirofit's B1200 rocket elbow stove, now discontinued, was chosen for the in-situ testing. The B1200 was used because it has a ceramic chamber, which is less susceptible to corrosion than a metal chamber, as it would be undesirable for the stoves themselves to degrade or fail during testing due to corrosive attack. Both stoves in their conditions prior to testing are shown in **Figure 3**.

Figure 3: *In-situ testing stoves prior to test. Stove A: left. Stove B: right.*

However, despite the precaution of using stoves with ceramic chambers, the bottom lining of the Stove B chamber slowly wore away during operation, and had to be replaced around 550 hours. This failure is discussed further in Chapter 3.

1.2.2 Lab furnace testing

Conditions inside a cookstove combustor are highly variable. Many factors are interdependent in how a stove operates and what conditions the combustor is exposed to. In particular, temperature and firepower vary with fuel feed rate and access to oxygen, which in turn are dependent on factors such as the operator, fuel type, and stove design [24], [25].

Corrosion rates and characteristics in a gas phase system are dependent on both the temperature of the metal and temperature of the gas [26]. Heat transfer between the metal and gas means the temperatures of these two media are interdependent. The system temperatures are affected by

factors such as fuel feed rate, air-fuel ratio, and insulation around the combustion chamber. In a stove that burns biomass fuels such as charcoal or wood, which are either batch fed (e.g. one load of charcoal equals one batch) or intermittently fed (e.g. by occasionally adding a stick to a wood stove), the environment inside the combustor never truly reaches a steady-state condition, and can be widely variable depending on factors such as fuel type and stove operator. In this project, these factors were kept as constant as possible. Fuel was kept consistent by maintaining the same fuel type and size throughout the testing, and always feeding the same number of sticks at a time. Stoves were always lit in the same manner. Stick spacing was managed by keeping the sticks so they were always touching each other. A total of about 10 people operated the stove over the course of the project, inherently introducing some variability into the stove operation method. However, all operators followed the same stove operation procedures.

The complexities of the biomass cookstove combustor environment indicate that the best way to predict the corrosion performance of a material when used as part of a cookstove combustor is to test it inside a cookstove. However, directly testing a material in a stove for a quantity of time that represents a substantial portion of the intended lifetime of the stove may be an unrealistic endeavor in many cases due to the time and labor required for testing, as someone must be physically present and operating the stove for the entire duration. In addition to accumulating exposure time, time must also be spent at regular intervals throughout the process to keep track of the coupons' progress. For example, in the in-situ test, stoves were stopped every 50 hours to remove coupons from the stove and weigh and photograph them. In this project, 1000 hours of in-situ exposure took around one year to complete.

Thus, the lab furnace test was developed as a simplified method that could approximate the temperature and atmosphere of a cookstove combustor but that could be completed much more quickly. While it does not perfectly simulate the conditions experienced inside a cookstove combustor, lab furnace testing is much less time and labor intensive than in-situ cookstove testing. The lab furnace method that was developed for this project is a simple procedure that could be easily implemented by parties wishing to quickly assess materials for cookstove combustors, and also could be used as a screening method to narrow down which materials to test by in-situ exposure. Lab furnace testing was completed at Oak Ridge National Laboratory and is discussed further in Chapter 3. One of the goals of this project was to evaluate the lab furnace test as a substitute and/or pre-screening method for the in-situ test.

CHAPTER 2: WOOD SALTING

2.1 Goal of salting process

Many types of biomass fuels can contain high quantities of salt species [19]–[21], [27] which can lead to accelerated corrosion [26], [28]–[30]. Chlorine in particular can lead to especially accelerated attack through the active oxidation mechanism [30]. Thus, salt was incorporated in both the in-situ and lab furnace test methods in order to (1) accelerate the corrosion and (2) simulate highly corrosive biomass fuels.

In the lab furnace test, the coupons were sprayed with a 3.5 wt% salt solution every 100 hours. In the in-situ test, the wood fuel was soaked in salt water prior to burning.

The salt used in both in-situ testing and lab furnace testing was Instant Ocean® Sea Salt, a commercial aquarium product with a composition meant to simulate the species in ocean water. The primary constituents of Instant Ocean® Sea Salt are Cl- and Na+, but the mix also contains a variety of other species. More details about the composition can be found in [31].

2.1.1 Halogen content testing method

The presence of salt in the fuel was quantified by measuring total halogen content. Halogen content analysis was performed by Huffman Laboratories, Inc. in Golden, Colorado. Samples were prepared at Huffman Laboratories by pulverizing the material to a fine powder before analysis. Samples were analyzed in duplicate. Results of total halogens (Cl + Br+ I) were reported as (µg halogen/g sample) and were given as equivalent chlorine. For wood fuels, a

cross-section of ~1/2-inch thickness by was cut from the middle of the 0.75” by 0.75” sticks for analysis.

2.2 Determination of target halogen content for fuel

A target halogen content for the fuel to be used for testing was identified by measuring the halogen content of two fuels that had been observed to be highly corrosive to cookstove combustors. The two fuels tested were mangrove lump charcoal from Haiti, with a halogen content of 760 µg halogen/g fuel, and Chabon Ticadaie Briquette Charcoal from Haiti, with 1390 µg halogen/g fuel. The average halogen content of these two fuels was 1075 µg/g. Thus, 1075 µg/g was used as a target value for halogen content of the lab-produced salted wood. These values are summarized in **Table 1**.

Table 1: *Target Halogen Content*

Fuel	**Halogen Content (µg/g)**
Mangrove lump charcoal	760
Chabon Ticadaie Briquette Charcoal (Haiti)	1390
Target Halogen Content (Average)	1075

2.3 Small-scale salting study

The wood used as fuel in the in-situ test was 0.75 in by 0.75 in pine trim purchased from Mawson Lumber and Hardware in Fort Collins, CO. This wood was chosen for its availability and because it is the wood with which small-stove testing is normally completed at CSU’s cookstoves lab. However, it is naturally low in halogen content, so the halogen content was increased artificially by soaking the wood in salt water.

The following procedure was used to estimate a target salt concentration of the water used for soaking the wood. Solutions of six different salt concentrations were created in 2-L mason jars. Each jar was filled with 1800 g of water and different quantities of salt. Seven-inch pieces of pine wood were dried in a kiln at 100 F for 3 days, then placed and sealed in the jars and allowed to soak for 11 days. Solution conductivity was measured every 2-3 days during the salting process using a CDM 80 Conductivity Meter (Radiometer Copenhagen). Jars are shown in **Figure 4.**

Figure 4: *Initial jar soaking study.*

After soaking for 11 days, the sticks from Jar A (highest salt) and Jar F (lowest salt) were removed from the jars for halogen testing. The sticks were cut in half and the halves used for testing were dried for 24 hours at 110 F then dried at 215 F for 72 hours. Contents of all jars, and halogen results for jars A and F are summarized in **Table 2**.

Table 2: *Salt concentration study – salt quantities and halogen results.*

Jar	Water Type	Water (g)	Salt (g)	Initial Conductivity (cell constant = 0.9)	Halogen Content (µg/g)
A	Tap	1800	75	30.20	11100
B	Tap	1800	37.5	16.67	--
C	Tap	1800	18.75	8.78	--
D	Distilled	1800	18.75	8.90	--
E	Tap	1800	9.37	4.77	--
F	Tap	1800	4.68	2.15	570

The goal behind measuring conductivity was that conductivity could be an indicator of salt concentration. A correlation between halogen content and conductivity was found so that, in theory, instead of measuring the mass or volume of water to determine the salt concentration, salt could be added to the water until the desired conductivity was achieved. It was determined by linear interpolation between Jar A and Jar F that, to achieve the target halogen content of 1000 µg/g, a conductivity of around 3.3 mS/cm was needed, as shown in **Figure 5.** More samples were not analyzed due to the cost of analysis.

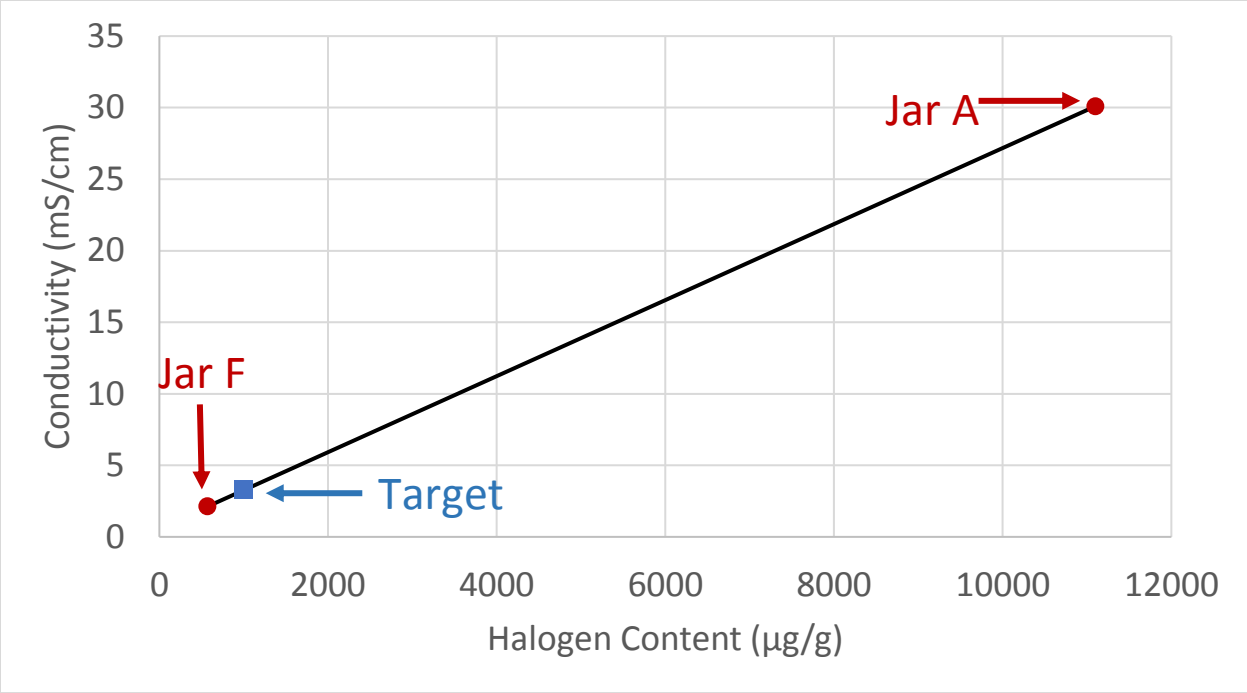

Figure 5: *Target conductivity for soaking water. Conductivity needed for target halogen content of 1000 µg/g was 3.3 mS/cm.*

It was found later that a direct correlation between initial conductivity and halogen content could not be made, discussed in section **2.6.3.**

2.4 Wood salting tanks

In order to produce fuel at a rate comparable to the rate at which it could be burned, the salting process was scaled up. Two salting tanks were constructed that could accommodate large batches of fuel. The first was a small 55-gallon tank, and the second was a 300-gallon tank.

2.4.1 Small-batch salting tank

Initial small batches of ~40 kg of salted wood were soaked in a 55-gallon polyethylene barrel. Sticks were cut to 24" and placed vertically in the barrel until the barrel was full, a total of ~200-300 sticks. To keep the wood submerged, a stainless steel plate, which was cut to fit inside the

barrel and which had holes to permit passage of water, was placed on top of the ends of the sticks, then bricks were place on top of the plate. Tap water was added to the barrel until the water level was above the stainless steel lid and 2-3" from the top, then salt was gradually added to the barrel. An 80 gal/hr pump with the inlet at the bottom of the barrel and outlet at the top of the barrel was included to help maintain uniform salt concentration throughout the barrel. The pump ran continuously. The wood soaked for a total of 12 days (Batch 1) to ensure that the tank had reached a state of equilibrium. The small-batch salting barrel with a load of wood after water was drained after soaking is shown in **Figure 6**.

Figure 6: *Small batch salting tank.*

The first three batches of wood were produced in the 55-gallon barrel, and all had finished soaking before burning started. The first batch of fuel (36 kg) was completely consumed after a total of 25 hours of burn time, which was accumulated over a period of 3 days. As it took a total of 17 days to process the same batch of wood, it was clear that the efficiency of the wood-salting process needed to be improved. Therefore, it was determined that the salting tank needed to be

even larger to accommodate a much larger batch of wood. The soaking time was also made shorter.

2.4.2 Large batch salting tank

The large-batch salting tank, shown in **Figure 7**, consisted of a 300-gallon plastic stock tank and a lid that was placed on top of the tank to keep the wood submerged.

Figure 7: *Large batch salting tank.*

The first step in the salting process was to fill the tank with wood. Stick length varied from 4 feet to 7 feet. Four-foot lengths were placed at the bottom of the tank where the tank was smaller, and 6-ft and 7-ft lengths were placed at the top where the tank was longer. Next, the lid was secured, and then the remainder of the volume inside the tank was filled with water. The tank was filled via hose. Total water volume was estimated by measuring the time to fill a 5-gallon bucket with

the hose, then comparing that value to the total time to fill the tank. Batches used ~180 gal of water on average. Salt was added at the end. Salt quantity was based on halogen content results from the first three batches and is discussed later in **Section 2.6.3**. A 185 gal/hr pump was placed at the bottom of the tank on the side before the tank was filled with wood. The pump circulated water continuously from the bottom to the top of the tank to encourage mixing of the water and promote uniformity of the salt concentration throughout the tank.

The conductivity meter was placed in the outlet of the pump, and conductivity of the water was monitored daily while the wood was soaking, in order to evaluate changes in salt absorption by the wood. As salt was absorbed by the wood, conductivity decreased. For the first large batch, when conductivity remained nearly constant over a period of ~3 days, it was determined that the wood/salt-water mixture had reached a state close to equilibrium, and the tank was drained. This occurred at a soaking time of ~5 ½ days. Subsequent batches were also drained after 5-6 days to keep a consistent soaking time across batches. Conductivity was also monitored in all batches to ensure it had reached a steady level at the end of soaking.

2.4.3 Buoyant force

Because the pine wood (measured density = 0.44 g/cm^3) was less dense than water (density = 1 g/cm^3), a means needed to be devised to counteract the buoyant force acting on the sticks in order to keep the wood submerged during soaking. The buoyant force is defined as the upward force acting on an object immersed in a fluid and is equal to weight of the fluid displaced by that object. The force that was needed to keep the wood submerged was equal to the difference between the buoyant force and the total weight of the wood.

In the 55-gallon barrel, the force needed was up to ~120 lb and was supplied by a stainless steel cover which was placed directly on top of the sticks. In addition, several bricks were placed on top of the stainless steel cover.

In the 300-gallon tank, the force needed was up to ~680 lb and was achieved by constructing a lid that was fixed to the tank with ratchet straps, and that had a lower section that dropped into the tank such that the level of the bottom of the lid was below the water level, thus keeping the wood completely submerged below the water level.

The lid consisted of a plywood sheet, which rested on top of the tank, and several 2x4" boards which were fixed to bottom of the plywood sheet such that they extended down below the top of the tank, and thus could keep the wood submerged as it soaked by pressing on the top of the batch of sticks. Front and side profiles of the lid are shown in **Figure 8**.

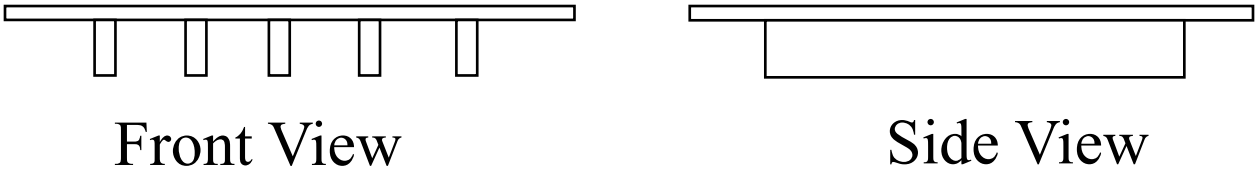

Figure 8: *Profile of salting tank lid.*

The tank sat on top of a pallet, under which two lengths of Unistrut were placed. The lid was secured to the tank by placing ratchet straps over the lid and fixing them to the Unistrut bars. Sections of steel angle were attached to the plywood's edges to prevent abrasion of the ratchet straps.

Thin particle board sheets were placed above the water on the sides of the tank in the areas that were not already covered by the main lid, in order to cover the water that was still exposed when the main lid was secured. The water was covered in an effort to reduce evaporation of the water as well as to prevent particles, e.g. sawdust, from falling into the water and accumulating.

2.5 Drying and cutting of wood

After the tank was drained, sticks were removed from the tank and stacked in alternating layers with space in between each stick to facilitate drying. After at least 2 days of drying in ambient air, the long (4-7ft) sticks were cut into 1-ft lengths, their final size. These short pieces were then dried in an oven set at 220^{o}F for an additional 2 days to remove any moisture that remained after air-drying, then put into storage.

2.6 Halogen content testing results

Samples from each batch were analyzed for halogen content to determine if the halogen content was close to the target value. Sticks tested for halogen content were randomly selected from each batch, with the exception of batch 3 – described in **Section 2.6.1.** Due to the high cost of analysis, only a small number of samples was analyzed for each batch. For several batches, only one sample was analyzed.

2.6.1 Effect of stick packing on halogen content – Batch 3

After Batch 3 finished soaking, samples were taken from various sticks in the batch to determine the effect of how closely packed sticks were on halogen content. Sticks were chosen both from the outside of the barrel where sticks were more exposed to water on their sides, and from the

inside where sticks were closely packed. Sticks from which samples were taken are those labeled and raised above the rest in **Figure 9**.

Figure 9: *Location of sticks from location/packing study.*

Results are summarized in **Table 3**.

Table 3: *Effect of stick packing on halogen content.*

	Outside #1	Outside #2	Inside #1	Inside #2	Inside #3, Compacted
Halogen Content (µg/g)	942	792	654	557	934

In this instance, it appeared that stick packing and location did not have any relationship to final halogen content. However, the sample size was small so more testing would be necessary to determine the true effect of stick location and packing on halogen content.

2.6.2 Effect of distance along stick on halogen content – Batch 4

To determine the effect of distance from the end of the stick on halogen content of the salted wood, halogen content was analyzed at different locations along a stick. A sample was taken every 1ft along a single 6-ft stick from Batch 4 (see **Figure 10**).

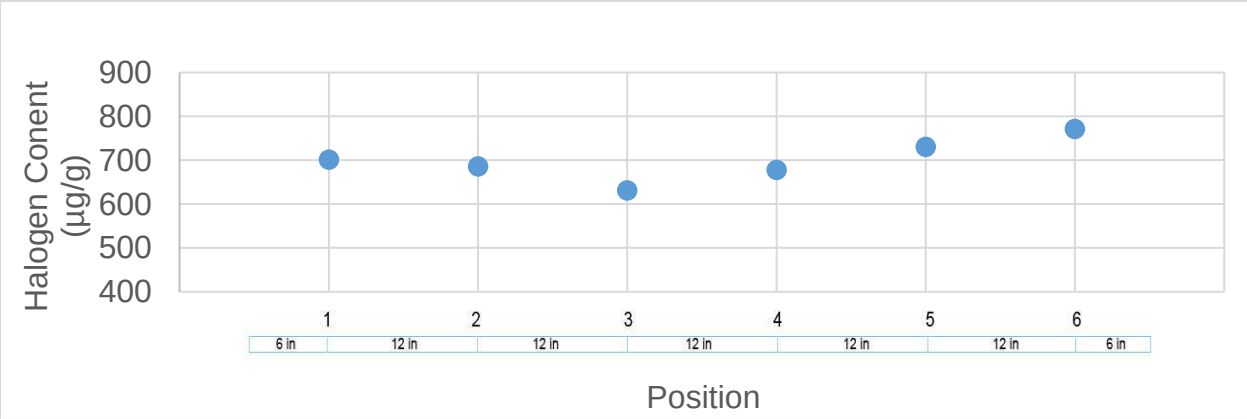

Figure 10: *Halogen content along a 6-ft stick after soaking for 6 days (Batch 4).*

As suspected, it was found that salt content was highest near the ends of the stick, and lowest in the middle. Halogen content results are given in **Table 4**.

Table 4: *Halogen content at different distances from the end of a 6-ft stick after soaking in salt water for six days (From Batch 4).*

Position	**1**	**2**	**3**	**4**	**5**	**6**
Distance from closest end of stick (in)	6	18	30	30	18	6
Halogen Content (µg/g)	701	686	631	678	730	771

Only one stick was analyzed; therefore, more testing would be necessary to determine a better representation of the effect of distance from the end of the stick on halogen content. However, it is interesting to note that there is less variability between samples from a single stick than samples from different sticks within a batch.

2.6.3 Batch-to-batch variation of halogen content

During the initial small-scale salting study, it was anticipated that the final halogen content of the wood could be predicted by the initial conductivity of the water. However, halogen content of the initial three batches came out lower than expected, at 281 µg/g, 650 µg/g, and 776 µg/g, indicating that the measure of conductivity alone cannot predict the final halogen content of the wood. It was suspected that this was due to the high ratio of wood to water in the tank. In the small-scale study, the ratio of wood to water is very low, and therefore, while some of the salt is moving from the water into the wood, that quantity of salt is small compared to the overall quantity of salt in the water. However, in the case of the large batches, when the volume ratio of wood to water is on the order of 0.5:1 to 1:1, if uptake of salt by the wood is disproportionately high compared to the uptake of water, then the overall salt concentration and conductivity of the water will decrease.

After discovering that conductivity could not be used as a measure for final halogen content in a large batch setting, a trial-and-error method was used for the subsequent batches. The salt concentration necessary for Batch 4 was estimated from the salt concentration of the first three batches, increasing the salt concentration proportionally, based on the ratio of measured halogen content to target halogen content. However, salt concentrations from Batches 1-3 were not known precisely since the water quantity in these batches was not measured.

Halogen content results from Batch 4 were also lower than desired, at 700 µg/g, so the salt content of the water for Batch 5 was further increased proportionally, based on the ratio of target halogen content to measured halogen content of Batch 4. Since the same process was used for

filling tank and the estimated volume of water in the tank was similar, it was assumed that batch 4 and 5 had similar quantities of water and wood, so the ratio was applied directly to the salt mass added.

Halogen content of sticks from batch 5 also came back lower than desired, at 821 µg/g, However, this value was within 20% of the target value and was closer to the target halogen content (~1000 µg/g) than the previous batches. In order to maintain a constant procedure for the following batches, the same quantity of salt as batch 5 was used for all subsequent salting batches. The method of filling remained constant for batches four through 10: the tank was filled with wood, the remainder of the volume in the tank was filled with water, and adding the given mass of salt at the end. Salt mass was different between batch 4 and 5, but was constant between batches 5-10. Water and wood quantities, and halogen content results from all batches are summarized in **Table 5.**

Table 5: *Halogen content of wood in all batches.*

Batch #	***Water (gal)***	***Salt (g)***	***Wood (kg)***	***Halogen Content (µg/g)***
1	36	400	36	281
2	34	400	40	650
3	33	350	42	776
4	150	3675	113	700
5	165	5250	192	821
6	190	5250	199	1780
7	180	5250	117	548
8	175	5250	218	781
9	197	5250	175	1550
10	197	5250	239	1275
Total	**1357**	**36325**	**1371**	
Weighted Average All Batches	169	4702	177	1072
Weighted Average* Batches 5-10	184	5250	198	1160
Std. Dev. Batches 5 - 10	13	0	44	485

* Soaking process was being developed during batches 1-5, and thus halogen content differed from batch to batch. The final salting process was used for batches 5-10, which accounted for 83% of the total wood used in the in-situ cookstove alloy corrosion testing.

2.7 Suggestions for future wood salting endeavors

There are several improvements that could be made to the salting process, which are described below. While improving the consistency of the salting process would improve the test overall, it should be noted that other factors, especially those that contribute to the temperature of the combustion environment, also create a significant effect on corrosion [26], [28], [29].

2.7.1 Measurement of wood quantity

In this project, consistency was achieved by following the same process for filling each tank with wood. Total mass of each batch was recorded in the log progressively as it was burned; however, the total mass of wood in a batch was not known until it was completely burned. Volume of wood could be estimated by the total volume of water used to fill the tank, but no changes could be made to the amount of wood in the tank at this point. Thus, the quantity of wood placed in the tank for each batch was not measured directly in any way as the tank was being loaded.

In hindsight, it would have been relatively quick and easy to record the volume of wood as it was being added to the tank, as dimensions of the wood were consistent and known. In this manner, exactly the same quantity of wood could have been added to the tank for each batch, and thus, quantities of water, salt, and wood would have been constant across all batches. Another method would be to use a high-capacity scale to weigh each bundle of fuel before placing it in the tank.

2.7.2 Moisture content

Drying the wood completely before soaking it to remove initial moisture content of the wood as a variable could improve results. However, this strategy would likely be impractical.

As an example, take two cases where the mass of salt, the volume of water, and the volume of wood are constant, but the initial moisture content of the wood is very high in one case but very low in the other. Assuming the salt concentration in the wood reaches equilibrium with the salt concentration in the water, the initial moisture content of the wood could affect the final salt content in the wood. In the case that the wood already has very high moisture, then the total water quantity in the system would be slightly higher, so for the same quantity of salt, the salt concentration would be slightly lower, resulting in a lower final halogen content of the fuel.

Drying the wood in advance of soaking could lower the variability in final halogen content, as any effects on salt absorption due to variability of moisture content could be avoided. However, reabsorption of moisture from the atmosphere could be highly variable depending on season and time between drying and soaking. Thus, fuel batches would have to be dried all at once, and would have to be moved immediately from drying into soaking in order to ensure that absorption of moisture from the air was minimized. Taking this into account, drying fuel before soaking in order to ensure constant initial moisture content may not be practical because it would be necessary to have an oven large enough to accommodate an entire batch of fuel (~200 kg for large batches).

CHAPTER 3: METHODS OF TESTING

3.1 Material selection and production

Several commercially produced alloys were tested, along with several developmental alloys that were produced at ORNL. For the developmental alloys, thermodynamic modeling was performed on materials of various chemical compositions in order to identify and narrow compositions that were most likely to be successful. A list of materials and their compositions is given in **Table 6**.

Table 6: *Analyzed compositions in wt. % of alloys tested, by inductively coupled plasma and combustion techniques. (Impurities <= ~0.05 wt. % not reported).*

	Fe	Ni	Cr	Al	Si	Mo	Mn	Ti	C	Other
FeCrAlSi	75.99		14.56	5	2.81		0.47	0.49	0.066	
FeCrSi	80.85		15.15		2.44		0.47	0.47	0.57	
Fe25CrAl	68.99		25.1	4.84	0.01			0.47	0.07	
FeCrAlY	73.04	0.12	20.42	5.65	0.24		0.18		0.016	0.05Y, 0.04Hf 0.05Zr
310S	53.23	18.83	25.17		0.59	0.43	0.91		0.03	0.3Cu 0.17Co 0.09V 0.06Nb
446	74.1	0.17	24.09		0.26		0.75		0.058	0.14V 0.11Nb
316L	67.86	9.98	17.08		0.43	2.1	1.56		0.026	0.46Cu 0.07V
201	70.73	4.42	16.21		0.5	0.26	6.79		0.085	0.71Cu 0.07Co 0.068N
AFA*-25Ni	51.83	25.04	13.84	3.56	0.13	0.18	1.99		0.114	2.51Nb 0.51Cu 0.16W
AFA*-20Ni	57.61	19.96	13.87	3.06	0.12	1.99	1.99		0.152	0.6Nb 0.52Cu
AFA*-12Ni	62.39	12.02	13.91	2.52	0.11	0.11	4.97		0.201	3.06Cu 0.59Nb
Pure Ni	0.09	99.44			0.04		0.23		0.068	0.06Co

*AFA = Alumina-Forming Austenitic

In addition to the standard FeCrAlY, a preoxidized commercial FeCrAlY was tested. The preoxidized FeCrAlY was FeCrAlY that was exposed in air at 1100 C for 2 hours, generating a thin alumina surface layer, before being introduced into lab furnace or in-situ testing.

3.2 Preparation of coupons

Material sample sheets were cut by electrical discharge machining (EDM) into coupons: test samples with dimensions of about 2.5 cm by 1.3 cm by .75 to 1.2 mm thickness. For the in-situ testing, a ~4 mm hole was the cut in the top of each coupon to be able to hang the coupon in the stove. For the lab furnace tests, coupons were cut to 20mm by 10 mm, by 0.75 to 1.2 mm thickness. No hole was cut for the lab furnace tests. Production of test coupons (performed by ORNL) is described in detail in the **Appendix B**. An example of a coupon before and after 250 hours of exposure in-situ cookstove test is shown in **Figure 11**.

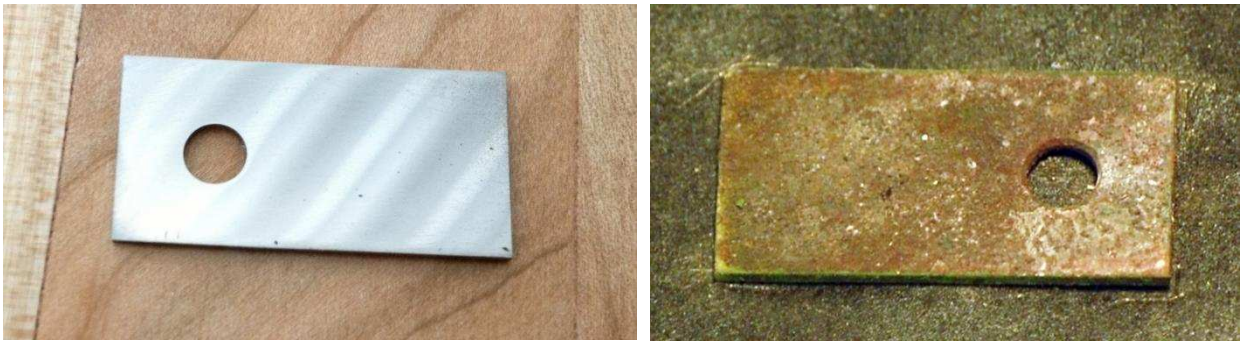

Figure 11: *Coupon prior to in-situ cookstove exposure, and after 250 hours. Material: Commercial FeCrAlY.*

Uncoated coupons were cleaned with acetone and isopropyl alcohol prior to exposure in order to ensure that no residual materials were present on the surface that could have an effect on material performance. Coated coupons were not cleaned before exposure. Nitrile gloves were worn at all times during coupon handling. Initial mass, length, width, thickness, and hole diameter were

measured before coupons were exposed. Coupon mass was recorded after every 50 hours of exposure. Length dimensions were not measured again until after exposure was completed, at which point cross-sections were cut, and intact metal thickness measurements were made under a microscope.

Length, width, and hole diameter were measured to a precision of 0.01 mm using digital calipers. Thickness was measured to the .001 mm using a digital micrometer. Thickness measurements were made at three different locations on each coupon (top, middle, and bottom) so that the initial thickness could be closely matched to the location where cross-sections were cut. See **Figure 12** for thickness measurement locations.

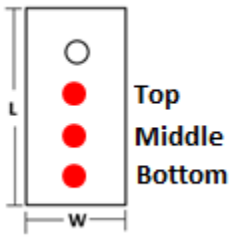

Figure 12: *In-situ cookstove testing: Locations of initial thickness, length and width measurements.*

3.3 Mass measurement of coupons

In the in-situ cookstove test, the mass of each coupon was measured to 1-microgram precision using a Mettler-Toledo MXS microbalance. A polonium-210 neutralizer was used to eliminate static from the items being measured.

After being exposed inside the cookstoves, oxides began to form on the surface of the coupons and therefore coupons could not be placed directly on the microbalance, as some of the corroded material was lost any time the coupons were handled. Thus, they were weighed in a plastic

weigh-boat that could capture any oxide scale that fell of the coupons during handling. The mass of the weigh-boat was measured, then a coupon was placed in the boat and the mass of (boat + coupon) was measured. Then the boat weight was subtracted from total weight. Weigh-boats were also used for initial weighing of coated coupons, but not for the initial weighing of uncoated coupons.

3.4 Demagnetization of coupons

During measurement of initial coupon mass, it was found that for some coupons, mass measurements were not repeatable. During experimentation to determine the cause of this problem, it was observed that even though measurements were highly variable, when a coupon was placed on one side, its average measured weight was significantly higher than when placed on the opposite side, as shown in **Figure 13**.

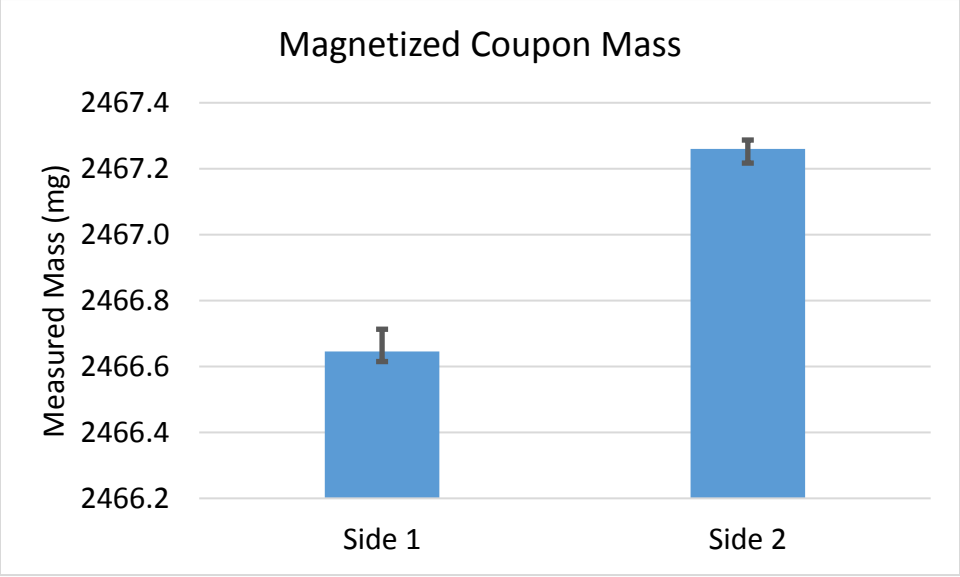

Figure 13: *Magnetization - measured mass of coupon when weighed on both sides. Error bars show range of measurements for each side. 14 measurements on each side.*

Thus, it was hypothesized that the coupons might be magnetized. At this point, all coupons were demagnetized using a Magnetizer/Demagnetizer (Kendrick & Davis, Syosset, NY). After demagnetization, the mass measurements of the coupons were consistent. Demagnetization was subsequently included in the initial procedure for all new coupons added to the test matrix.

3.5 In-stove fixtures for in-situ testing

To allow direct exposure of material samples to combustion products for the in-situ portion of the test, fixtures from which coupons could be hung were fabricated and placed inside of each stove. The fixtures were designed to hang coupons inside the stoves such that they would be directly exposed to the flame and would also be located near the hottest part of the combustion chamber, in order to simulate the exposure that a combustion chamber itself would receive. Each fixture was supported by its top flange, which rested on the top of the pot supports of each stove. The body of the fixture hung inside the chimney, and held coupons at the base of the chimney, as shown in **Figure 14**.

Figure 14: *Fixture for hanging coupons inside stove.*

Each fixture held three coupon hangers, and each hanger could hold up to 5 coupons. Thus, each fixture could accommodate up to 15 coupons at a time. With two stoves, the total capacity for exposure was 30 coupons at a time. The fixtures and hangers were constructed using Hastelloy X, a material shown to have excellent high temperature corrosion resistance and fabricability. Coupons in fixtures can be seen in **Figure 15**.

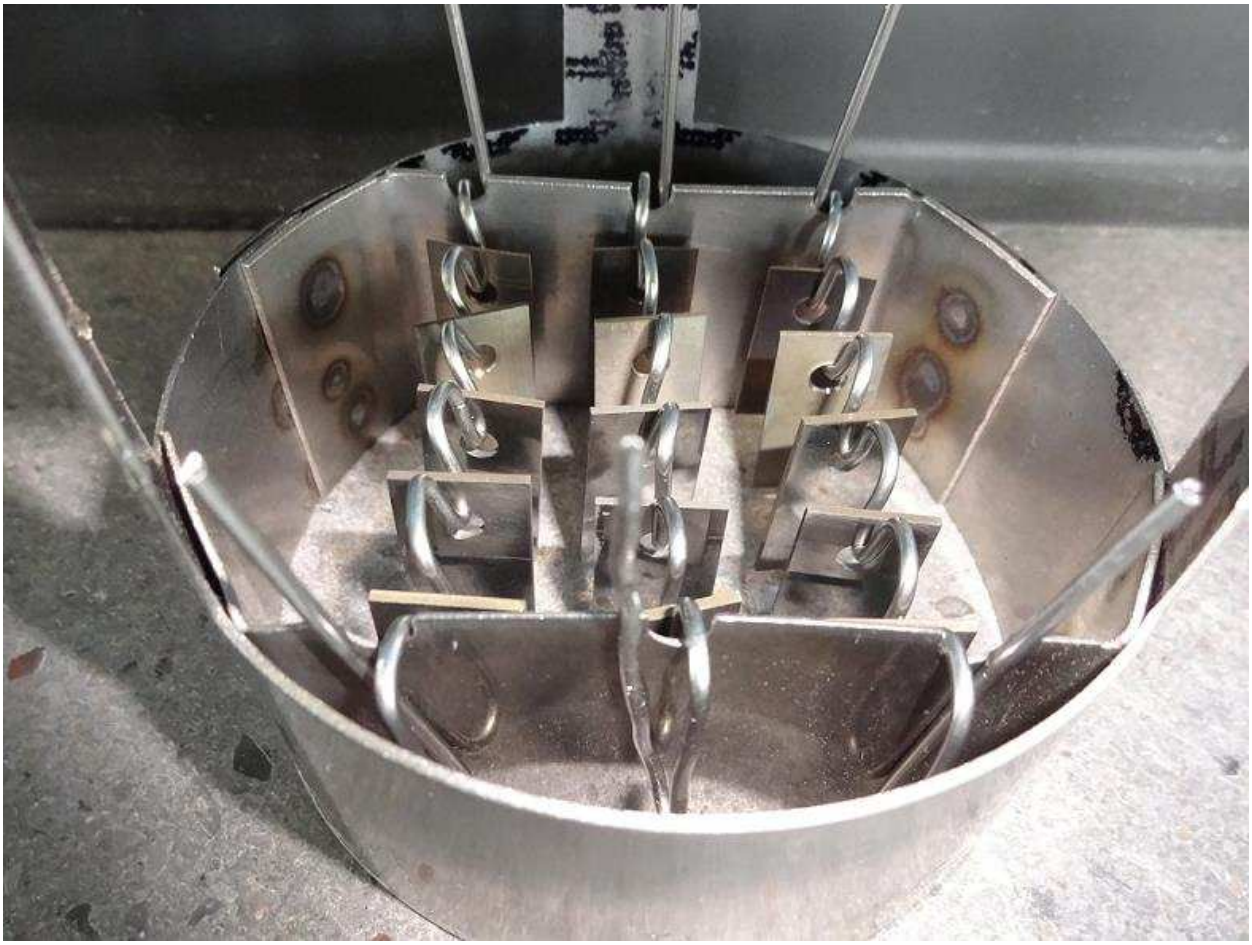

Figure 15: *Fixture with coupons before exposure.*

Stoves and fixtures were engraved for identification. The coupons themselves could not be engraved or otherwise labeled, as corrosion during the test could yield the coupons unidentifiable. Thus, a method to identify the coupons needed to be developed. A set of six distinct hangers was created, shown in **Figure 16**.

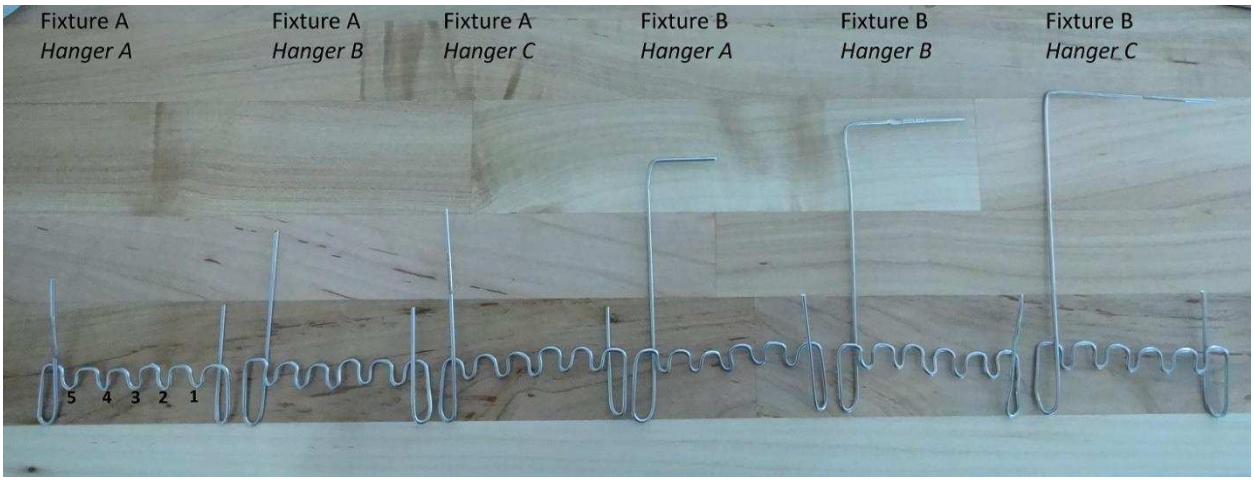

Figure 16: *Hangers used for in-situ testing*

Each had the same pattern in the region that was supporting the coupons; however, the ends of the hangers were cut to different lengths. Each hanger had a long side and a short side to differentiate between the ends of the hangers. The long end of each hanger was cut to a different length from the others in order to differentiate among the hangers. The long end of each of the hangers for stove B was bent inward at a 90-degree angle to differentiate between the Stove A hangers and the Stove B hangers. In this way, any coupon could be identified by its position on the hanger when the hangers were removed from their fixtures in the stove. A schematic of coupon positions is shown in **Figure 17**.

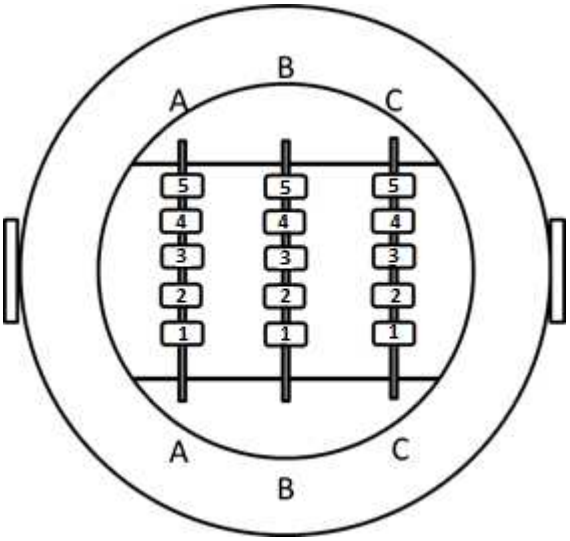

***Figure 17**: Schematic identifying coupon locations within fixture.*

3.6 Operation of cookstoves

3.6.1 Operational process and run schedule

Stoves were burned for in-situ testing according to the following procedure.

Each stove was started using two unsalted pine shim packs. When the shim packs had burned about halfway, three salted pine sticks were loaded into the stove. Sticks used in testing were 0.75” by 0.75” by 12”. New sticks were fed three at a time, and each new stick was placed so that it was in line with the stick ahead of it. The stove feeding process is illustrated in **Figure 18**.

Figure 18: *Startup of stove using shim packs, transition from shim packs to sticks, and transition from one set of sticks to the next.*

After every 2-3 sets of sticks were consumed, the char that had accumulated in the chamber was removed with a steel spoon. Each day of testing, stoves were burned continuously for an average of 6 hours. A log was kept to track the duration and mass of fuel consumed each time the stoves were burned. After every 50 hours of cumulative exposure time, the coupons were removed from the stove then weighed and photographed. Both sides of each coupon were photographed.

Testing took place over the course of 15 months. The total number of days that the stoves were operated was 195 days. The stoves were operated for a total of 1150 hours for the in-situ portion of the testing.

3.6.2 Stick spacing

Stick spacing and is an important variable that influences measures of stove performance [32] and also affects the burn rate of fuel and temperature in cookstoves. During startup, to facilitate lighting of the fuel, sticks were loaded with ~1/2" of space between them. However, after the

combustor had reached normal operating temperature, in order to reduce variability in burn rate and combustor temperature due to stick spacing, sticks were kept so they were always touching (zero stick spacing).

3.6.3 Rotation of fixtures

In the stoves used for in-situ testing, the flame was visibly stronger and temperatures were higher at the back of chimney than at the front. Therefore, a rotation scheme was introduced in an effort to expose the coupons more evenly. Every hour of exposure, the fixture holding the coupons in each stove was rotated 90 degrees clockwise.

3.7 Unsalted wood testing

In addition to the testing with salted fuel, some coupons were tested with unsalted fuel in order to compare the corrosion resulting from salted fuel to the corrosion resulting from unsalted fuel. The total exposure time with unsalted fuel was 150 hours. The burning process was the same as for salted fuel, and was completed after the main salted wood burning. Differences were clear even after this short time and are discussed further in **Section 5.6**.

3.8 Limiting factors for accumulation of exposure time

Several factors became limiters to the speed of operation of this testing that caused delays in the exposure process. These factors were: wood availability, soaking time, and drying time. It was anticipated that drying time would be the limiting factor for the rate at which exposure time could be accumulated, so an oven was purchased for additional drying capacity. However, in the end, the most limiting factor was the soaking time.

- Wood availability – wood was purchased in large orders that frequently had a large time between ordering and arrival.
- Wood soaking - the entire wood soaking process took approximately 9-10 days to complete for the large batches. This time included cutting fuel and loading it into the tank, draining the tank after soaking, removing the fuel and stacking it to be dried, and letting the fuel air dry for at least two days then cutting it into 1-ft lengths before drying it in the oven or kiln for an additional two days. The duration of the process was even longer for the small batches when the soaking time was longer.
- Wood drying – The oven and kiln could only accommodate a fraction of a batch at a time, so the oven and kiln needed to be loaded several times to completely dry a batch of wood. Additionally, each load of fuel put into the oven or kiln was dried for 2 days before being removed.

3.9 Stove B failure and repair

During testing, the chamber of stove B slowly wore away, eventually and gradually exposing the metal bottom of the stove, which proceeded to corrode once it became exposed. Eventually, a hole developed in the metal bottom and the stove needed to be repaired after 550 hours of

exposure time. Because the B1200 was out of production, Stove B could not be replaced with a new stove.

Stove B was repaired by removing the remainder of the ceramic in the degraded chamber, and replacing it with the bottom ceramic tile of a different stove. The circular ceramic bottom combustion chamber liner of an Envirofit G3300 stove was cut to the shape of the inside of the Stove B chamber using a waterjet cutter. Stove B, before and after repair, is shown in **Figure 19**.

Figure 19: *Stove B before testing (left), at 550 hours - before repair (middle), and after repair (right).*

To ensure that the operation of the Stove B was not significantly affected after replacing the bottom tile, temperature profiles of Stove A and B were recorded while the stoves were operated as similarly as possible. A thermocouple was placed in each stove near the bottom back of the chimney, directly in the flame zone. It was placed at the same level as the coupons, and thus experienced the same temperatures as the coupons would experience. The comparison of temperature profiles is shown in **Figure 20**.

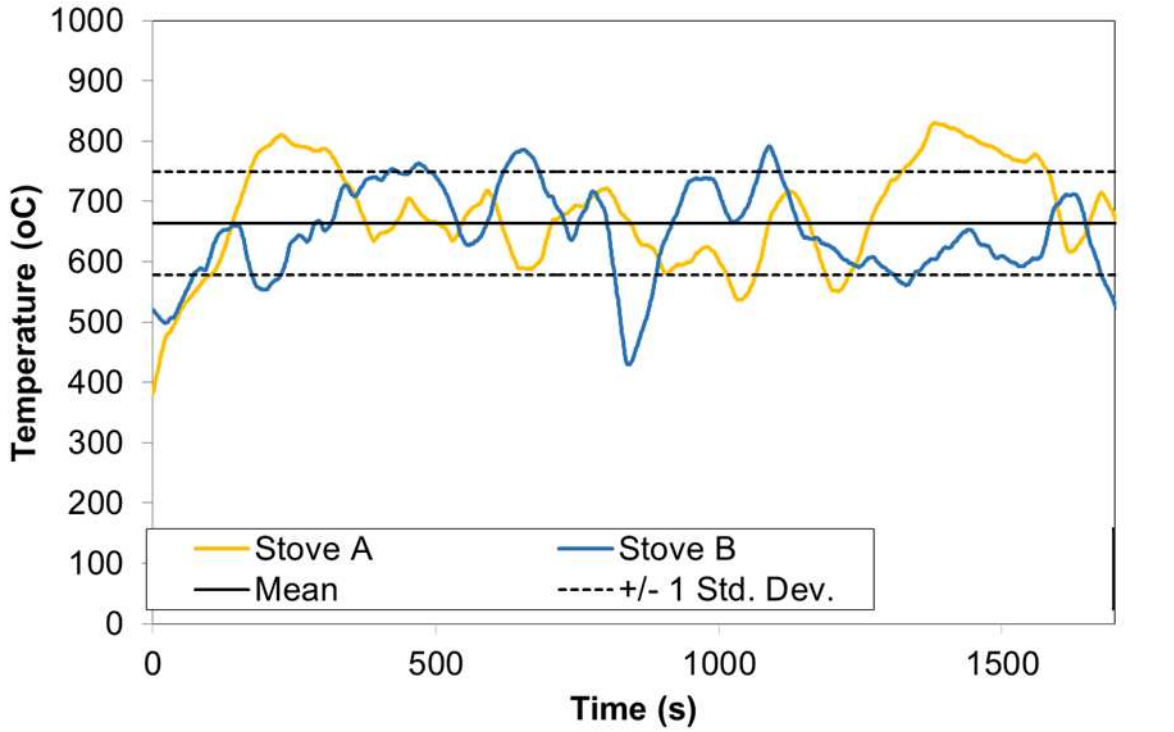

Figure 20: *Temperature profiles inside stove chimneys after repair of Stove B.*

It can be seen that the temperatures of the stoves were very similar to each other. During the test, Stove A had a mean temperature of 677ºC with a standard deviation of 85ºC, and stove B had a mean temperature of 650ºC with a standard deviation of 79ºC. The difference in mean temperature between stoves was only 34% of the standard deviation of stove B, and thus, it was determined that stove B produced adequately similar temperatures to stove A for the exposure of coupons to proceed.

As an additional check to the temperature profiles, three more control coupons were added to the in-situ test after stove B was repaired: one coupon in stove B at 550 hours, immediately after the repair, and one coupon each in stove A and stove B at 600 hours. Coupons' mass changes were recorded for the remainder of the test. Stove B was repaired at 550 hours but a coupon was added

to each stove simultaneously at 600 hours since Stove A was at its full capacity until 600 hours. In addition, a control coupon was put in stove B at 550 hours and also compared. Mass change of these coupons is shown in **Figure 21**.

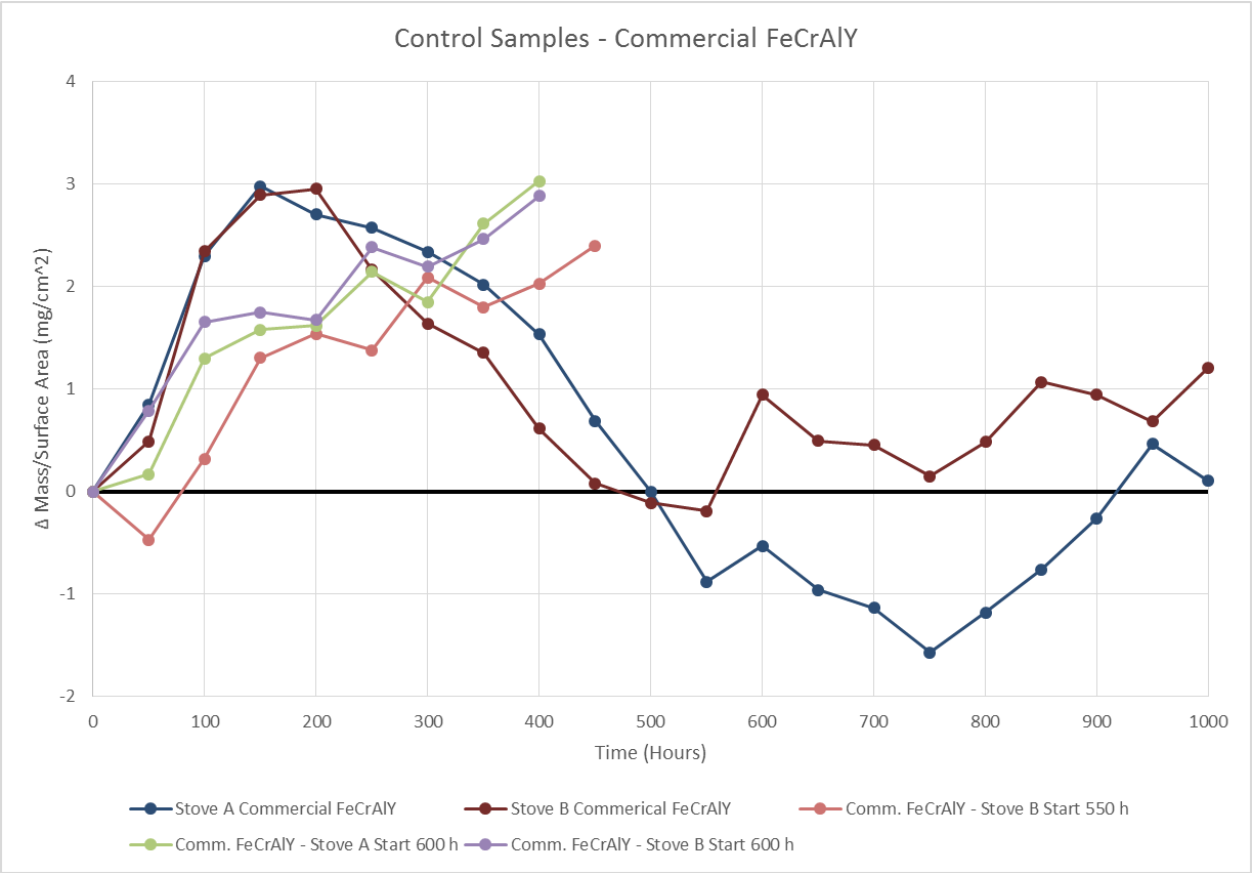

Figure 21: *In-situ testing mass change of control coupons.*

It is interesting that the stove B chamber degraded with time, while the Stove A chamber remained intact and relatively undamaged throughout the test. The stoves came from different production runs, and perhaps this contributed to the difference in the durability of the two stoves. One thought was that the chamber may have cracked, enabling a point of weakness where small pieces/chunks could be broken off in the process of removing char from the chamber.

3.10 Lab furnace testing

Lab furnace testing was completed as a means of testing that could simulate cookstove exposure but that be completed much more quickly than the in-situ cookstove test. Lab furnace testing was completed at Oak Ridge National Laboratory. In the lab furnace test, coupons were placed in a tray and a 3.5 wt% salt solution was sprayed on top of the coupons and then dried. The solution was sprayed only on the top face. The solution used Instant Ocean® Sea Salt and distilled water.

Two sets of furnace tests were competed: one with the furnace at 600^{o}C, and one at 800^{o}C. These values were chosen to span the range of temperatures a cookstove combustor is likely to experience. The atmosphere in the furnace was air with 10% volume of water vapor. This composition was used to simulate the water vapor produced during biomass combustion.

Coupons were removed every 100 hours for mass measurements, and the salt solution was reapplied before coupons were returned to the furnace for the next cycle. Three samples of each material were exposed. One sample was removed for cross-section analysis after 100 hours, the second removed after 500 hours, and the third removed after 1000 hours. Cross-section were cut and analyzed at ORNL. More details about lab furnace testing can be found in [23].

CHAPTER 4: METHODS OF EVALUATION

4.1 Specific mass change

One method by which corrosion was measured was by determining the mass change per surface area (specific mass change) of the coupons over time. Specific mass change was used instead of raw mass change in order to normalize for differences in coupon size. Total surface area was calculated from the initial length, width and thickness measurements. Mass change was determined by measuring the mass of the coupons periodically - every 50 hours for the in-situ cookstove test and every 100 hours for the lab furnace test. The mass change quantities were divided by the initial total surface area of the coupons to find the specific mass change.

Measuring mass change enables non-destructive evaluation of corrosion; however, mass change alone does not give an accurate indication of corrosion resistance. High mass change, either in the positive or negative direction, is an indication that the material is performing poorly. Formation of oxides results in an increase in mass, and oxide flaking or volatilization results in a mass loss. However, a combination of oxide formation and oxide loss can result in low net mass change. Additionally, the metal may be falling victim to internal grain boundary attack without a large change in mass. Thus, specific mass change alone cannot give a full picture of corrosion.

.

4.2 Cross-sectional analysis

To thoroughly asses the corrosion resistance of a material, it is necessary to perform cross-sectional analysis to visually assess the material to determine the types of attack and how far the corrosion has penetrated.

After exposure in either lab furnace or in-situ testing, coupons were removed for cross-section analysis, performed at Oak Ridge National Laboratory. Cross-section analysis was destructive, and thus coupons could not be returned to testing after analysis. Three samples of each material were exposed in each test scenario (600^{o}C lab furnace, 800^{o}C lab furnace, and in-situ cookstove test). One was removed at 100 hours, another at 500 hours, and the third at 1000 hours. After removal from testing, a cross-section was cut by low speed diamond saw. Corrosion was quantified in terms of material loss by comparing the initial thickness to the thickness of intact metal remaining. The thickness of intact metal was defined at the point at which the metal did not show signs of internal attack.

4.2.1 Cross-sectional analysis method

Cross sections were prepared at oak Ridge National Lab, as described below:

> "Exposed test samples were cross-sectioned by low-speed diamond saw and prepared by standard metallographic techniques (oil based rather than aqueous polishing media was used to avoid dissolution of possible chloride and related corrosion products during sample preparation). The cross-sections were analyzed by light microscopy, scanning electron microscopy (SEM) with energy dispersive x-ray spectroscopy (EDS), and electron probe microanalysis (EPMA) using both EDS and wavelength dispersive spectroscopy (WDS). Initial sample thickness was measured with a micrometer. Cross-section thickness measurements of corroded samples were made using an optical measurescope (light microscope with digitized micrometer stage measurement attachment). The test sample cross-sections along the 10-12.5 mm sample width were divided into 3 regions, not including 1 mm from the sample end corners. In each of the 3 sample regions, the area of greatest corrosion attack was selected for measurement of intact metal remaining in cross-section. The boundary

of the intact metal was defined as the point at which the underlying metal was free of oxide scale and internal attack. The average of the three locations of greatest attack was used to plot metal loss vs. time" [23].

CHAPTER 5: RESULTS AND DISCUSSION

5.1 Mass change and material loss results

In the in-situ cookstove test, exposure proceeded for a total of 1150 hours. The in-situ cookstove test could only accommodate 30 coupons at a time. Thus, some materials could not begin exposure until other samples had been removed for cross-section analysis. Hence, AFA 25 Ni, AFA 20Ni, AFA 12 Ni, 201 stainless, and Pure Nickel started exposure 500 hours after the other materials began, and thus could only accumulate 650 hours by the end of the test period. All materials were exposed for 1000 hours in the 600ºC furnace test, except for pure nickel, which was exposed for 500 hours. In the 800ºC furnace test, seven materials were exposed for 1000 hours, and six were exposed for 500 hours. A summary of exposure times is shown in **Table 7**.

Table 7: *Exposure times of materials in lab furnace and in-situ testing.*

	Exposure Time (hours)		
Material	**600ºC Lab Furnace**	**800ºC Lab Furnace**	**In-situ Cookstove**
201	1000	500	500
316L	1000	500	1000
446	1000	500	1000
310S	1000	1000	1000
FeCrAlY	1000	1000	1000
Preox FeCrAlY	1000	1000	1000
FeCrAlSi	1000	1000	1000
FeCrSi	1000	1000	1000
25Cr FeCrAl	1000	1000	900
AFA 25Ni	1000	500	650
AFA 20Ni	1000	500	650
AFA 12Ni	1000	500	650
Pure Ni	500	1000	650

5.1.1 600ºC lab furnace test results

In the 600ºC furnace test, after 1000 hours, metal loss ranged from 10 µm to 330 µm. Specific mass change was in the range of 5 mg/cm^2, with the exception of 201 stainless, which showed a specific mass change of -50 g/cm^2. Among the commercial alloys, FeCrAlY and preoxidized FeCrAlY showed the highest corrosion resistance, with metal losses of 20 µm and 10 µm, respectively, and mass changes of 1.2 mg/cm^2 and 0.7 mg/cm^2, respectively. The commercial alloy that displayed the lowest corrosion resistance was 201 stainless, with metal loss of ~240 µm, and mass change of -50 mg/cm^2. The AFAs also showed high cross-sectional metal loss, even though they showed low specific mass change. FeCrAlSi, FeCrSi and 25Cr-FeCrAl showed the best corrosion resistance among the developmental alloys, all with metal loss of ~30 µm, and mass changes of 0.7 mg/cm^2, 0.8 mg/cm^2, and 0.9 mg/cm^2, respectively. Results from the 600ºC furnace test are shown in **Figure 22**.

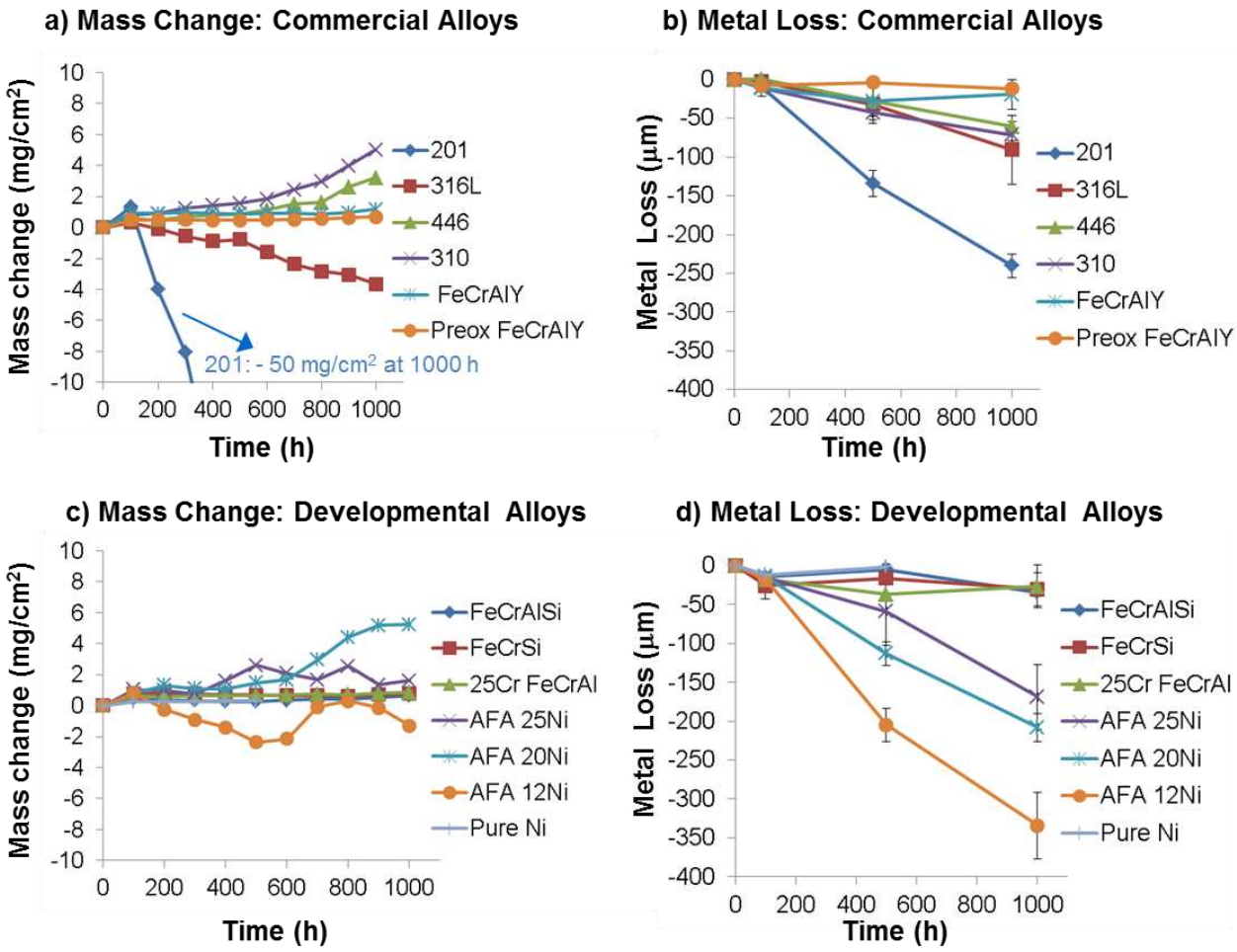

Figure 22: *Corrosion data from 600°C lab furnace testing. Metal loss data plotted as the average ±1 standard deviation of the 3 locations of greatest attack. The environment was air + 10% H2O, with salt added at the start of testing and re-applied after every 100 h cycle.*

5.1.2 800ºC lab furnace test results

The 800ºC furnace test yielded much faster corrosion rates than the 600ºC lab furnace test. Many alloys were removed after 500 hours in the 800ºC furnace test due to poor performance (201, 316L, 446, AFA 25Ni, AFA 20Ni, and AFA 12Ni). Of the materials that were exposed to 1000 hours, metal loss ranged from 140 µm to 1000 µm and mass change ranged from -31.6 mg/cm^2 to 1.4 mg/cm^2. FeCrSi and Pure Ni performed the best with metal losses of 160 µm and 140 µm, respectively, and mass changes at 1000 hours of -1.5 mg/cm^2 and -0.01 mg/cm^2, respectively. Results from the 800ºC furnace test are shown in **Figure 23**.

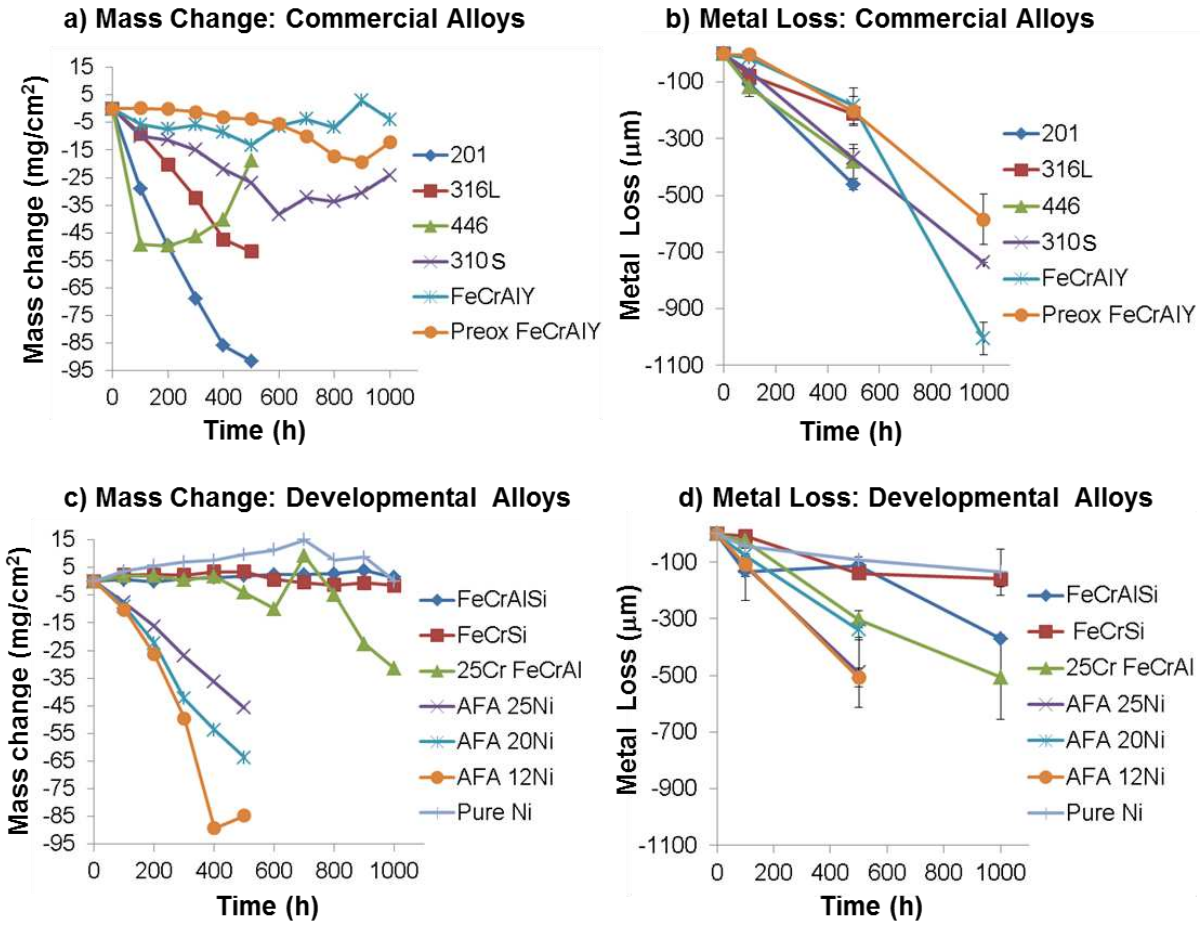

Figure 23: *Corrosion data from 800ºC lab furnace testing. Metal loss data plotted as the average ±1 standard deviation of the 3 locations of greatest attack. The environment was air + 10% H2O, with salt added at the start of testing and re-applied after every 100 h cycle.*

While in the 600ºC test, the best-performing commercial alloys and developmental alloys showed similar metal loss, there was a notable difference between the best developmental alloys and the best commercial alloys in the 800ºC furnace test. In terms of metal loss, the best-performing developmental alloy, FeCrSi (metal loss = 160 µm), performed substantially better than the best-performing commercial alloy, Preoxidized FeCrAlY (metal loss = 580 µm).

5.1.3 In-situ cookstove test results

For the in-situ test, metal losses ranged from 100 µm to 370 µm, and mass changes ranged from -60.7 mg/cm^2 to 5.3 mg/cm^2. Mass change plots clearly show high corrosion rates in 201, 316L, and 446, and these alloys also showed the highest metal losses from cross-section analysis. As in the 800ºC furnace test, the best-performing commercial alloys were FeCrAlY and preoxidized FeCrAlY, with metal losses of 110 µm and 100 µm, respectively, and mass changes of 0.1 mg/cm^2 and -3.9 mg/cm^2, respectively. The best performing developmental alloys were FeCrSi and FeCrAlSi, with metal losses of 117 µm and 100 µm, respectively. In-situ cookstove test results are shown in **Figure 24**.

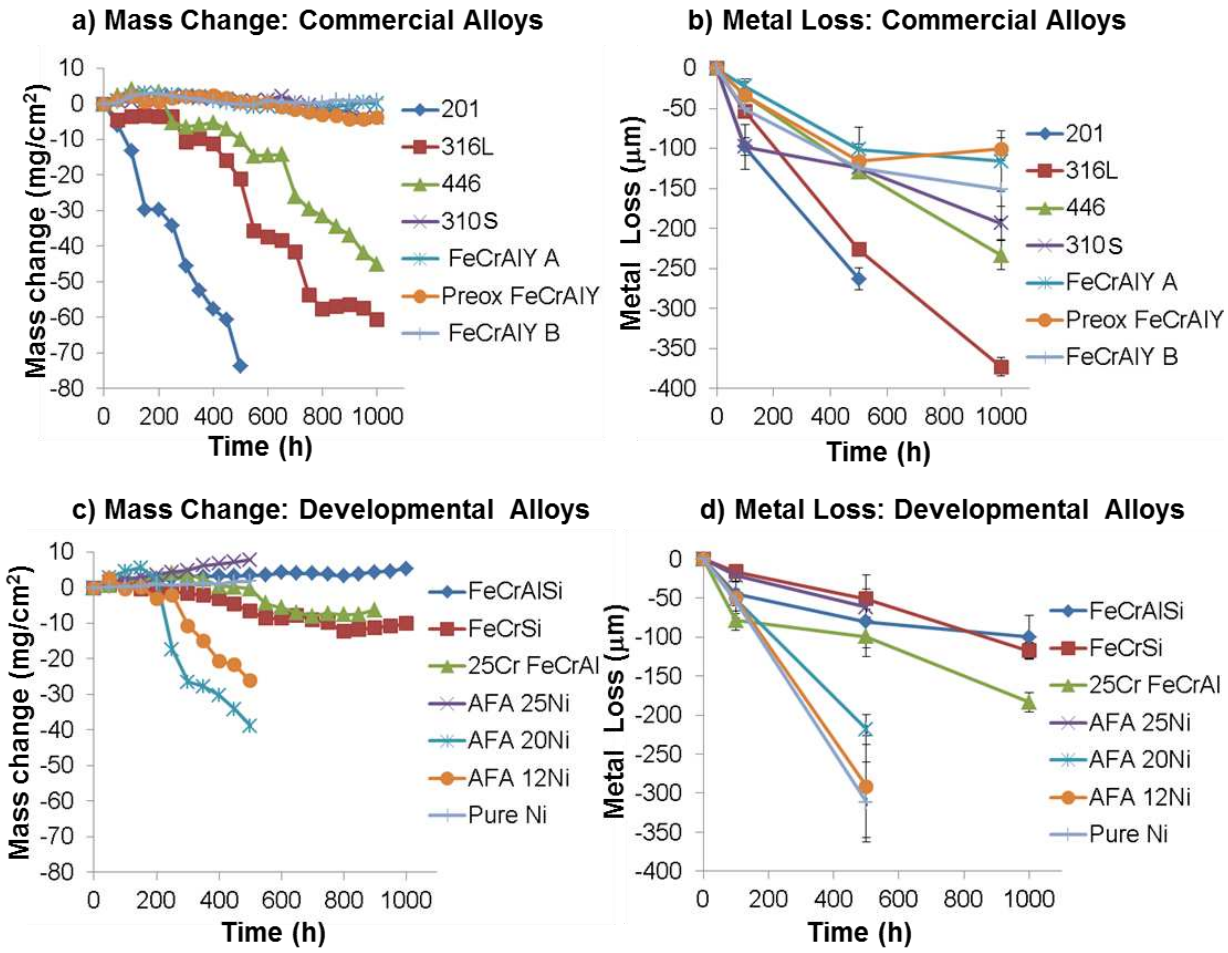

Figure 24: *Corrosion data from in-situ cookstove testing. Metal loss data plotted as the average ±1 standard deviation of the 3 locations of greatest attack. FeCrAlY A and FeCrAlY B are duplicate samples run in each of the two cookstove test beds utilized. Salted pine wood was burned to induce accelerated corrosion conditions.*

5.2 Comparison between tests

Similar corrosion performance trends amongst the alloys were evident across all three tests. Additionally, corrosion rates in the in-situ test were intermediate between the rates observed in the 600ºC and 800ºC lab furnace tests, which is consistent with the average stove temperature of ~663ºC. The exception was that while Ni showed the highest corrosion resistance in both lab furnace tests, with 500-hour metal losses of 2 µm and -93 µm in the 600ºC and 800ºC lab furnace tests, respectively, it experienced much more corrosion in the in-situ test, with metal loss

of -300 µm after 500 hours. This could be because of a difference in the species present between tests. There could have been species present in biomass combustion that were not present in the lab furnace test that contributed to the more severe attack of nickel in the in-situ test.

Alloys were ranked relative to each other qualitatively based on mass change, metal loss, and cross-section microstructure features, as displayed in **Table 8**.

Table 8: *Qualitative ranking of relative corrosion resistance of alloys in the 3 conditions studied. Most corrosion resistant listed at top, least at bottom. Multiple alloys listed in the same table cell indicate similar levels of corrosion resistance.*

In-Situ Cookstove	**600°C Lab Furnace**	**800°C Lab Furnace**
FeCrAlY, Pre-oxidized FeCrAlY, FeCrAlSi, FeCrSi	Pure Ni, Pre-oxidized FeCrAlY	Pure Ni, FeCrSi
AFA-25Ni, 310S, 446, 25Cr-FeCrAl	FeCrAlY, FeCrAlSi, FeCrSi, 25Cr- FeCrAl	FeCrAlSi
316L, 201, AFA-20Ni	446, 310S, 316L	25Cr-FeCrAl, FeCrAlY, Pre-oxidized FeCrAlY,
AFA-12Ni, Pure Ni	AFA-25Ni, AFA-20Ni	316L, 446, 310S
	201	201, AFA-25Ni, AFA-20Ni, AFA-12Ni
	AFA-12Ni	

A quantitative comparison between the metal loss results is shown in **Figure 25**, below.

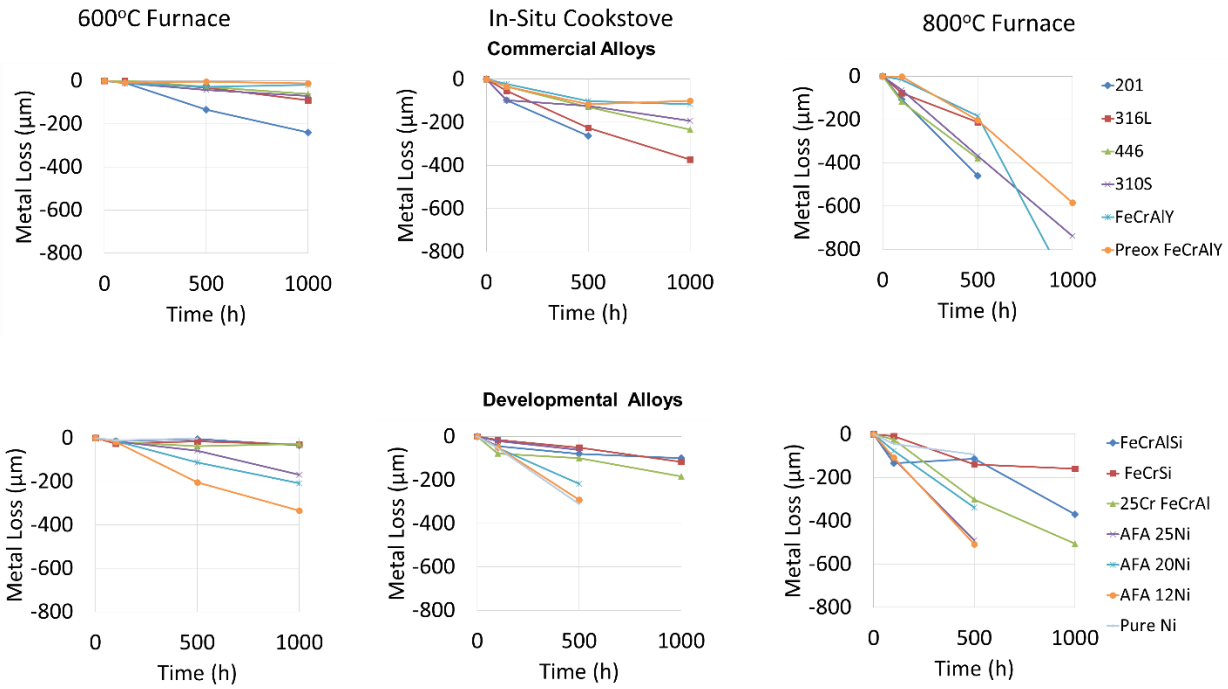

Figure 25: *Metal loss results for 600 C lab furnace, in-situ cookstove, and 800 C lab furnace tests.*

5.3 Comparison with field sample

A sample of 310S from a cookstove used in the field that showed extensive corrosion was compared with samples of 310S exposed in the in-situ cookstove test and in the 600°C and 800°C lab furnace tests. Cross sections were compared at Oak Ridge National Laboratory, as seen in **Figure 26**.

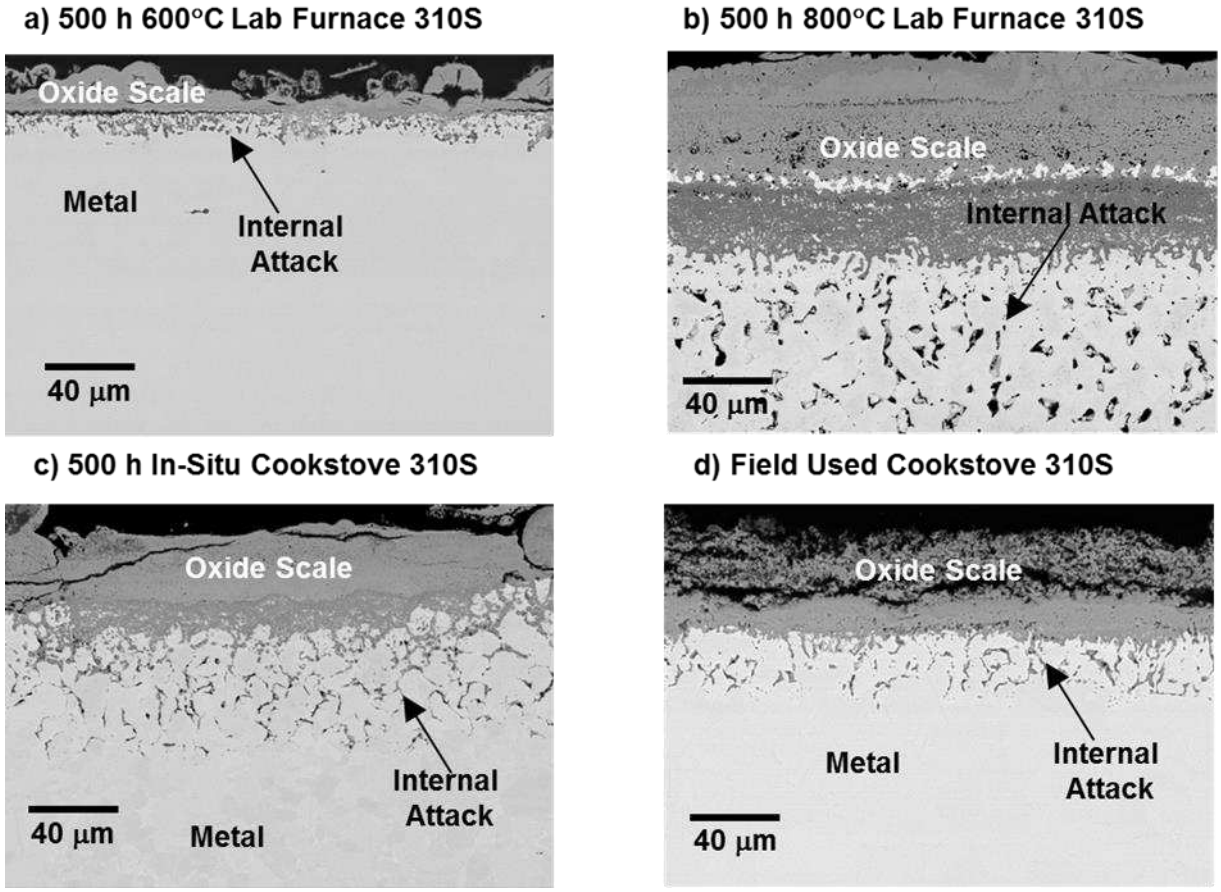

Figure 26: *Cross-section backscatter mode SEM images of 310S stainless steel after 500 h exposure in (a) 600°C lab furnace testing, (b) 800°C lab furnace testing, and (c) in-situ cookstove testing. A cross-section of a 310S combustor from a field-operated cookstove is shown in (d) for comparative purposes.*

All samples had the same characteristics of internal attack in addition to a non-protective oxide scale. These similarities indicate that both the lab furnace and in-situ cookstove tests can be useful as material screening tests by approximating the corrosive conditions that can be found in cookstoves used in the field.

5.4 Importance of cross section analysis

The behavior of 310S exemplifies the need for cross-sectional analysis for measurement of metal loss - even if a material is showing low mass change, it may be succumbing to internal corrosion

that is not evident from mass measurements alone. While the mass change of 310S was one of the lower mass changes among the materials, at -3.8 mg/cm^2 after 1000 hours in the in-situ cookstove test, the metal loss as determined by cross section measurement was -233 µm, which was the second-highest metal loss value for the 1000-hour in-situ cookstove test.

5.6 Salted vs. Unsalted Results

After 1000 hours, there were only 11 coupons remaining in the test. Thus, with a capacity of 15 coupons per stove, only one stove needed to be burned for all coupons to be exposed to salted wood combustion. At this point, Stove A continued to be burned with salted wood while Stove B was burned with unsalted wood, and one new sample of the control material, Commercial FeCrAlY, was placed in each stove.

As can be seen in the mass change plot in **Figure 27**, the corrosion rate of the sample follows a parabolic trend for the case of unsated wood, likely indicative of a protective oxide layer.

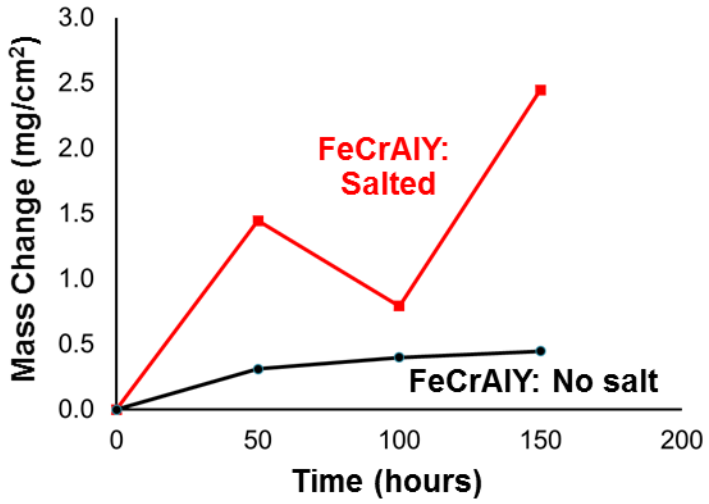

Figure 27: *Mass change for the commercial FeCrAlY alloy from in-situ cookstove testing using as-received pine wood and salted pine wood.*

On the other hand, for the case of salted wood, the mass change is higher, and the alternating increases and decrease suggests that the oxide layer is growing and periodically spalling off. These results indicate that the salted wood is effectively creating harsh, corrosive conditions, conducive to accelerating the material testing process.

5.5 FeCrSi Alloy

The FeCrSi alloy showed the highest level of corrosion resistance. An additional benefit of FeCrSi is that it has the potential to be produced at a lower cost than FeCrAl alloys and austenitic alloys considered to be state-of the art for cookstove combustors. The factor that led to its success was that FeCrSi was the only material that did not exhibit internal attack. The corrosion resistance of FeCrSi was particularly evident in the 800^{o}C lab furnace test. For example, while FeCrAlY performed well in the lower temperature tests, it showed through-thickness internal attack in the 800^{o}C furnace test. **Figure 28** gives a comparisn of 310S, FeCrAlY, and FeCrSi after 1000 hours in the 800^{o}C furnace test.

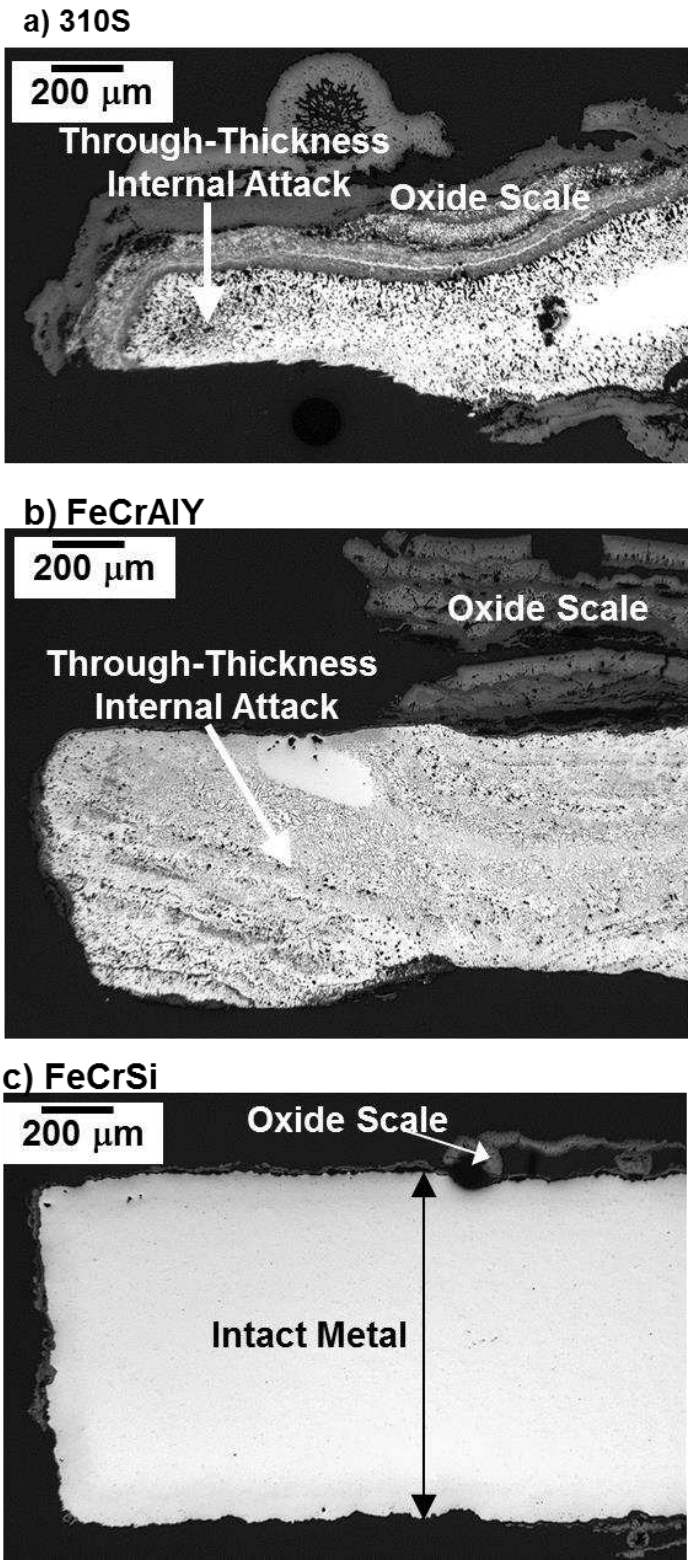

Figure 28: *Cross-section light microscopy images after 1000 h of lab furnace testing at 800°C for (a) 310S, (b) FeCrAlY, and (c) FeCrSi*

One reason that has been postulated for why additions of Si increase the corrosion resistance is that Si can lead to increased diffusivity of Cr, which is beneficial for the formation of a more protective Cr_2O_3 scale [15], [16]. Another reason is that the presence of Si can enable the formation of a thin layer of SiO_2 at the interface between the metal and the scale that provides additional defense against corrosive attack [14], [17].

CHAPTER 6: CONCLUSIONS

6.1 Wood salting

A method for producing salted wood by soaking it in salt water was established. The halogen content of the wood can be varied by changing the salt concentration in the water. However, salt concentration in the water is not the only variable that will affect the halogen content of the wood. The relative ratios of water, salt, and wood are all important in determining the final halogen content in the wood. Additionally, halogen content can be highly variable even within a single batch of salted wood.

6.2 Lab furnace and in-situ testing

Burning salted wood successfully created highly corrosive conditions that were much more corrosive than when unsalted wood was burned, indicating that soaking wood in salt water to add salt content is an effective way to accelerate corrosion for in-situ cookstove testing.

In-situ cookstove testing provides the most accurate evaluation cookstove combustor materials; however, a simplified lab furnace test can be completed much more quickly, and provides a good proxy for exposure conditions inside cookstoves. The lab furnace test is not as representative of actual cookstove conditions and operation, and therefore the in-situ cookstove testing is a better representation of how materials would perform in the field. However, lab furnace testing can be a simple way to approximate the conditions inside a cookstove combustor for the purpose of evaluating a material's corrosion resistance in cookstoves applications.

Similarities in corrosion between lab furnace, in-situ, and field material samples indicate that both the lab furnace and in-situ tests can be effective accelerated-corrosion screening tests for evaluating corrosion performance of materials in a cookstove setting.

6.3 Material identification

An FeCrSi alloy was identified as a material that could be very successful for the application of improved biomass cookstoves, with both a substantially higher corrosion resistance, and a potentially lower cost to produce. FeCrSi was among the highest performers in all three tests (600^{o}C furnace, 800^{o}C furnace, and in-situ). The lack of internal attack is an indication of this alloy's success; FeCrSi did not suffer from internal attack, while all other materials tested did. The formation of protective Cr_2O_3 and SiO_2 oxide layers are likely what contribute to its increased corrosion resistance.

Before use in a cookstove combustor application, the FeCrSi alloy needs to be evaluated for mechanical properties, manufacturability, and weldability. The FeCrSi alloy also needs to be tested for corrosion resistance in the field.

If this alloy is successful in manufacturability and field testing, then it is a strong candidate as a material that can address the issues of both affordability and durability: two important factors for achieving widespread improved biomass cookstove adoption.

6.4 Relative material behavior and cost versus corrosion resistance

One manner in which the topic of durability and affordability of materials could be approached is from the perspective of balancing material thickness, corrosion resistance, and cost in such a way that long stove lifespans could be achieved. For example, one could potentially increase the lifetime of a stove by increasing the thickness of the material used in the combustor. In this way, one could theoretically compensate for the low corrosion resistance of a low-cost material by increasing the thickness of the material. If the cost of a material is sufficiently low, a case could be made from the material cost perspective that it could be better to use a greater thickness of a cheaper material rather than a lesser thickness of a more corrosion resistant but costlier material.

However, such a concept has a number of shortcomings. First, increased material thickness could be detrimental to stove performance. More material would mean a greater thermal mass, and thus, more energy would need go into the stove to heat the stove up, potentially decreasing the thermal efficiency. Second, corrosion rates are not necessarily linear. Corrosion rates of materials that form protective oxide layers will decrease with time; on the other hand, corrosion rates can be linear with time if the material forms a non-protective oxide layer [12]. Third, field conditions are different from experimental conditions and vary between stove users. Taking these considerations together, it would not be straightforward to translate the experimental results into an accurate projection of stove lifetime in the field.

While precise quantification of corrosion resistance is difficult, the experiments performed in this study do provide a comparison between the relative corrosion performance of different

materials, and a strong indication as to which materials offer the greatest corrosion resistance. In this way, this research can act as an aide for stove manufacturers in material selection.

REFERENCES

[1] S. Bonjour *et al.*, "Solid fuel use for household cooking: Country and regional estimates for 1980-2010," *Environ. Health Perspect.*, 2013.

[2] "World Health Organization Fact sheet No 292 Household air pollution and health," *WHO*, 2016. [Online]. Available: http://www.who.int/mediacentre/factsheets/fs292/en/. [Accessed: 24-Feb-2017].

[3] M. Ezzati and D. M. Kammen, "The health impacts of exposure to indoor air pollution from solid fuels in developing countries: Knowledge, gaps, and data needs," *Environ. Health Perspect.*, vol. 110, no. 11, pp. 1057–1068, 2002.

[4] F. Lacey and D. Henze, "Global climate impacts of country-level primary carbonaceous aerosol from solid-fuel cookstove emissions," *Environ. Res. Lett.*, vol. 10, no. 11, p. 114003, 2015.

[5] A. P. Grieshop, J. D. Marshall, and M. Kandlikar, "Health and climate benefits of cookstove replacement options," *Energy Policy*, vol. 39, no. 12, pp. 7530–7542, 2011.

[6] K. R. Smith, R. Uma, V. V. N. Kishore, J. Zhang, V. Joshi, and M. a K. Khalil, "G REENHOUSE I MPLICATIONS OF H OUSEHOLD S TOVES : An Analysis for India," *Annu. Rev. Energy Environ.*, pp. 741–763, 2000.

[7] M. P. Kshirsagar and V. R. Kalamkar, "A comprehensive review on biomass cookstoves and a systematic approach for modern cookstove design," *Renewable and Sustainable Energy Reviews*. 2014.

[8] C. Venkataraman, A. D. Sagar, G. Habib, N. Lam, and K. R. Smith, "The Indian National Initiative for Advanced Biomass Cookstoves: The benefits of clean combustion," *Energy Sustain. Dev.*, vol. 14, no. 2, pp. 63–72, 2010.

[9] I. Ruiz-Mercado, O. Masera, H. Zamora, and K. R. Smith, "Adoption and sustained use of improved cookstoves," *Energy Policy*, vol. 39, no. 12, pp. 7557–7566, 2011.

[10] S. Baldwin, "Biomass Stoves, Engineering Design, Development and Dissemination," 1987.

[11] M. P. Brady, I. G. Wright, and B. Gleeson, "Alloy design strategies for promoting protective oxide-scale formation," *Jom*, vol. 52, no. 1, pp. 16–21, 2000.

[12] W. J. W. Donald R. Askeland, Pradeep P. Fulay, *The Science and Engineering of Materials*, 6th ed. 2011.

[13] K. H. Lo, C. H. Shek, and J. K. L. Lai, "Recent developments in stainless steels," *Mater. Sci. Eng. R Reports*, vol. 65, no. 4–6, pp. 39–104, 2009.

[14] Y. S. Li, Y. Niu, and M. Spiegel, “High temperature interaction of Al/Si-modified Fe-Cr alloys with KCl,” *Corros. Sci.*, vol. 49, no. 4, pp. 1799–1815, 2007.

[15] H. J. Grabke, M. Spiegel, and A. Zahs, “Role of Alloying Elements and Carbides in the Chlorine-Induced Corrosion of Steels and Alloys 89 Role of Alloying Elements and Carbides in the Chlorine-Induced Corrosion of Steels and Alloys,” *Mater. Res.*, vol. 7, no. 1, pp. 89–95, 2004.

[16] M. Spiegel, A. Zahs, and H. J. Grabke, “Fundamental Aspects of Chlorine Induced Corrosion,” *Mater. High Temp.*, vol. 20, no. 2, pp. 153–159, 2003.

[17] Y. S. Li, M. Spiegel, and S. Shimada, “Effect of Al/Si addition on KCl induced corrosion of 9% Cr steel,” *Mater. Lett.*, vol. 58, no. 29, pp. 3787–3791, 2004.

[18] M. P. Brady, J. Magee, Y. Yamamoto, D. Helmick, and L. Wang, “Co-optimization of wrought alumina-forming austenitic stainless steel composition ranges for high-temperature creep and oxidation/corrosion resistance,” *Mater. Sci. Eng. A*, 2014.

[19] R. A. Antunes and M. C. L. de Oliveira, “Corrosion in biomass combustion: A materials selection analysis and its interaction with corrosion mechanisms and mitigation strategies,” *Corrosion Science*. 2013.

[20] L. L. Baxter *et al.*, “The behavior of inorganic material in biomass-fired power boilers: field and laboratory experiences,” *Fuel Process. Technol.*, vol. 54, pp. 47–78, 1998.

[21] R. Saidur, E. A. Abdelaziz, A. Demirbas, M. S. Hossain, and S. Mekhilef, “A review on biomass as a fuel for boilers,” *Renewable and Sustainable Energy Reviews*. 2011.

[22] S. C. Okoro, M. Montgomery, F. J. Frandsen, and K. Pantleon, “Effect of Water Vapor on High-Temperature Corrosion under Conditions Mimicking Biomass Firing,” *Energy and Fuels*, vol. 29, no. 9, pp. 5802–5815, 2015.

[23] M. P. Brady *et al.*, “Alloy Corrosion Considerations in Low-Cost, Clean Biomass Cookstoves for the Developing World,” *Energy Sustain. Dev.*, vol. 37, 2017.

[24] C. L’Orange, M. DeFoort, and B. Willson, “Influence of testing parameters on biomass stove performance and development of an improved testing protocol,” *Energy Sustain. Dev.*, vol. 16, no. 1, pp. 3–12, 2012.

[25] J. Tryner, B. D. Willson, and A. J. Marchese, “The effects of fuel type and stove design on emissions and efficiency of natural-draft semi-gasifier biomass cookstoves,” *Energy Sustain. Dev.*, vol. 23, no. 1, pp. 99–109, 2014.

[26] G. Sorell, “The role of chlorine in high temperature corrosion in waste-to-energy plants,” *Mater. High Temp.*, 1997.

[27] S. V. Vassilev, D. Baxter, L. K. Andersen, and C. G. Vassileva, “An overview of the chemical composition of biomass,” *Fuel*. 2010.

[28] H. P. Nielsen, F. J. Frandsen, K. Dam-Johansen, and L. L. Baxter, “Implications of chlorine-associated corrosion on the operation of biomass-fired boilers,” *Prog. Energy Combust. Sci.*, 2000.

[29] D. A. Tillman, D. Duong, and B. Miller, “Chlorine in solid fuels fired in pulverized fuel boilerss-sources, forms, reactions, and consequences: A literature review,” *Energy and Fuels*. 2009.

[30] H. J. Grabke, E. Reese, and M. Spiegel, “The effects of chlorides, hydrogen chloride, and sulfur dioxide in the oxidation of steels below deposits,” *Corros. Sci.*, 1995.

[31] M. J. Atkinson and C. Bingman, “Elemental composition of commercial seasalts,” 1997.

[32] K. Dischino, “Methods for particulate matter emissions reduction in wood burning cookstoves,” 2015.

APPENDIX A: SUPPLEMENTAL TABLES AND FIGURES

Table 9: Small-scale salting study: conductivity over time

			Conductivity (mS/cm)					
Date	Water Temp (C)	Cell Constant (cm^-1)	Jar A	Jar B	Jar C	Jar D	Jar E	Jar F
2/6/2014 *before sticks	21	0.9	30.2	16.67	8.78	8.90	4.77	2.15
2/7/2014	20	0.9	30.4	16.74	8.73	8.89	4.76	2.14
2/10/2014	22	0.9	30.3	16.63	8.72	8.88	4.76	2.12
2/12/2014	23	0.9	30.2	16.61	8.71	8.88	4.76	2.12
2/14/2014	23	0.9	30.2	16.61	8.72	8.88	4.77	2.12
2/17/2014	23	0.9	30.1	16.58	8.71	8.89	4.77	2.12

Table 10: 600ºC Furnace Test Metal Loss Results – Commercial Alloys

		Metal Loss (µm)					
Time (h)		201	316L	446	310S	FeCrAlY	Preox FeCrAlY
0	Avg	0	0	0	0	0	0
	Std. dev.	0	0	0	0	0	0
100	Avg	-9	-2	0	-11	-11	-8
	Std. dev.	3	3	4	5	8	3
500	Avg	-134	-32	-28	-43	-28	-4
	Std. dev.	17	4	20	9	20	2
1000	Avg	-240	-90	-61	-71	-19	-12
	Std. dev.	15	45	7	7	2	1

Table 11: 600°C Furnace Test Metal Loss Results – Developmental Alloys

		Metal Loss (µm)						
Time (h)		FeCrAlSi	FeCrSi	25Cr FeCrAl	AFA 25Ni	AFA 20Ni	AFA 12Ni	Pure Ni
0	Avg	0	0	0	0	0	0	0
	Std. dev.	0	0	0	0	0	0	0
100	Avg	-15	-26	-18	-15	-14	-18	-12
	Std. dev.	4	17	7	4	1	6	3
500	Avg	-5	-16	-37	-59	-113	-205	-2
	Std. dev.	7	8	23	43	16	21	2
1000	Avg	-34	-30	-27	-169	-208	-334	
	Std. dev.	5	21	27	42	18	43	

Table 12: 800°C Furnace Test Metal Loss Results – Commercial Alloys

		Metal Loss (µm)					
Time (h)		201	316L	446	310S	FeCrAlY	Preox FeCrAlY
0	Avg	0	0	0	0	0	0
	Std. dev.	0	0	0	0	0	0
100	Avg	-107	-78	-118	-63	-16	-2
	Std. dev.	11	16	32	10	6	2
500	Avg	-460	-212	-380	-368	-184	-203
	Std. dev.	19	21	60	32	63	51
1000	Avg				-738	-1006	-584
	Std. dev.				0	58	90

Table 13: 800°C Furnace Test Metal Loss Results – Developmental Alloys

		Metal Loss (µm)						
Time (h)		FeCrAlSi	FeCrSi	25Cr FeCrAl	AFA 25Ni	AFA 20Ni	AFA 12Ni	Pure Ni
0	Avg	0	0	0	0	0	0	0
	Std. dev.	0	0	0	0	0	0	0
100	Avg	-133	-8	-25	-114	-76	-108	-44
	Std. dev.	103	11	2	35	4	21	7
500	Avg	-113	-139	-302	-489	-339	-508	-93
	Std. dev.	20	23	31	124	35	33	10
1000	Avg	-371	-159	-506				-136
	Std. dev.	7	26	149				81

Table 14: In-situ cookstove test metal loss results – commercial alloys

		Metal Loss (µm)						
Time (h)		201	316L	446	310S	FeCrAlY A	FeCrAlY B	Preox FeCrAlY
0	Avg	0	0	0	0	0	0	0
	Std. dev.	0	0	0	0	0	0	0
100	Avg	-98	-54	-33	-98	-22	-34	-51
	Std. dev.	11	2	17	28	9	5	5
500	Avg	-263	-226	-129	-124	-101	-116	-125
	Std. dev.	14	5	9	14	28	22	9
1000	Avg		-373	-233	-193	-116	-101	-151
	Std. dev.		12	18	21	38	14	37

Table 15: In-Situ Cookstove Test Metal Loss Results – Developmental Alloys

		Metal Loss (µm)						
Time (h)		FeCrAlSi	FeCrSi	25Cr FeCrAl	AFA 25Ni	AFA 20Ni	AFA 12Ni	Pure Ni
0	Avg	0	0	0	0	0	0	0
	Std. dev.	0	0	0	0	0	0	0
100	Avg	-45	-16	-79	-21	-52	-50	-53
	Std. dev.	7	6	12	8	24	20	7
500	Avg	-80	-51	-100	-62	-218	-291	-311
	Std. dev.	33	13	25	41	19	65	52
1000	Avg	-100	-117	-183				
	Std. dev.	28	10	12				

Table 16: 600ºC Furnace Test Specific Mass Change Results – Commercial Alloys

	Specific Mass Change (mg/cm2)					
Time (h)	**201**	**316L**	**446**	**310S**	**FeCrAlY**	**Preox FeCrAlY**
0	0.00	0.00	0.00	0.00	0.00	0.00
100	1.30	0.33	0.58	0.79	0.90	0.49
200	-4.02	-0.07	0.50	0.90	0.91	0.49
300	-8.04	-0.56	0.69	1.24	0.96	0.50
400	-15.97	-0.89	0.78	1.41	0.92	0.48
500	-19.06	-0.77	0.87	1.57	0.88	0.48
600	-24.54	-1.61	1.13	1.84	0.94	0.49
700	-30.29	-2.36	1.50	2.44	0.91	0.53
800	-35.26	-2.82	1.63	2.97	0.84	0.54
900	-40.80	-3.05	2.59	3.98	0.97	0.62
1000	-52.28	-3.67	3.22	5.01	1.17	0.69

Table 17: 600ºC Furnace Test Specific Mass Change Results – Developmental Alloys

	Specific Mass Change (mg/cm2)						
Time (h)	**FeCrAlSi**	**FeCrSi**	**25Cr FeCrAl**	**AFA 25Ni**	**AFA 20Ni**	**AFA 12Ni**	**Pure Ni**
0	0.00	0.00	0.00	0.00	0.00	0.00	0.00
100	0.44	0.79	0.62	1.05	0.78	0.82	0.23
200	0.36	0.75	0.60	0.99	1.31	-0.25	0.26
300	0.32	0.77	0.62	0.76	1.09	-0.90	0.27
400	0.28	0.70	0.63	1.60	1.11	-1.39	0.29
500	0.28	0.68	0.64	2.61	1.49	-2.36	0.29
600	0.34	0.67	0.70	2.09	1.67	-2.14	
700	0.43	0.67	0.75	1.66	2.95	-0.09	
800	0.43	0.63	0.72	2.56	4.41	0.30	
900	0.55	0.71	0.80	1.34	5.17	-0.14	
1000	0.65	0.76	0.86	1.61	5.24	-1.29	

Table 18: 800°C Furnace Test Specific Mass Change Results – Commercial Alloys

	Specific Mass Change (mg/cm2)					
Time (h)	**201**	**316L**	**446**	**310S**	**FeCrAlY**	**Preox FeCrAlY**
0	0.00	0.00	0.00	0.00	0.00	0.00
100	-29.03	-9.04	-49.25	-9.99	-5.80	0.20
200	-49.70	-20.17	-49.74	-11.31	-7.43	-0.19
300	-68.89	-32.42	-46.38	-14.92	-5.96	-1.26
400	-85.97	-47.43	-40.24	-22.09	-8.55	-3.19
500	-91.53	-51.74	-18.74	-26.84	-13.32	-3.82
600				-38.40	-6.29	-5.62
700				-32.16	-3.79	-10.05
800				-33.66	-6.85	-17.29
900				-30.45	2.93	-19.27
1000				-24.17	-3.98	-12.23

Table 19: 800°C Furnace Test Specific Mass Change Results – Developmental Alloys

	Specific Mass Change (mg/cm2)						
Time (h)	**FeCrAlSi**	**FeCrSi**	**25Cr FeCrAl**	**AFA 25Ni**	**AFA 20Ni**	**AFA 12Ni**	**Pure Ni**
0	0.00	0.00	0.00	0.00	0.00	0.00	0.00
100	0.53	2.26	1.89	-7.78	-9.08	-10.30	3.69
200	-0.23	2.35	1.88	-16.29	-22.41	-26.48	5.55
300	1.07	2.31	0.44	-27.01	-42.49	-49.50	6.87
400	1.40	3.51	1.78	-36.41	-53.73	-89.16	7.48
500	1.99	3.53	-4.06	-45.69	-63.76	-84.71	9.58
600	2.35	0.61	-9.91				11.35
700	2.39	-0.41	9.14				14.88
800	2.77	-1.35	-4.87				7.73
900	3.96	-0.55	-22.70				8.79
1000	1.37	-1.46	-31.55				-0.01

Table 20: In-Situ Cookstove Test Specific Mass Change Results – Commercial Alloys

	Specific Mass Change (mg/cm2)						
Time(h)	**201**	**316L**	**446**	**310S**	**FeCrAlY A**	**Preox FeCrAlY**	**FeCrAlY B**
0	0.00	0.00	0.00	0.00	0.00	0.00	0.00
50	-6.15	-4.66	2.34	0.98	0.85	1.07	0.49
100	-13.25	-3.49	4.14	0.51	2.30	2.00	2.34
150	-29.68	-3.43	2.89	0.96	2.97	0.69	2.89
200	-29.68	-3.64	3.25	1.29	2.70	0.62	2.95
250	-34.20	-3.62	-5.26	1.76	2.57	1.49	2.16
300	-45.66	-10.80	-6.52	2.11	2.33	2.08	1.64
350	-52.42	-9.65	-5.91	1.67	2.01	2.00	1.35
400	-57.59	-11.33	-5.18	1.45	1.53	2.33	0.61
450	-60.75	-15.94	-7.10	1.29	0.68	1.62	0.08
500	-73.84	-21.21	-10.06	0.81	0.00	0.68	-0.11
550		-35.72	-14.64	0.75	-0.88	0.32	-0.19
600		-37.48	-14.43	1.14	-0.53	0.42	0.94
650		-38.50	-14.30	2.19	-0.96	-0.78	0.49
700		-41.58	-25.96	0.42	-1.14	-1.53	0.45
750		-53.67	-29.47	-0.39	-1.57	-2.25	0.15
800		-57.60	-31.54	-2.17	-1.18	-3.17	0.48
850		-56.85	-34.55	-1.75	-0.76	-3.34	1.07
900		-56.56	-36.91	-2.18	-0.26	-4.24	0.94
950		-57.46	-41.75	-3.85	0.46	-4.38	0.68
1000		-60.70	-44.98	-3.79	0.10	-3.91	1.21

Table 21: In-Situ Cookstove Test Specific Mass Change Results – Developmental Alloys

	Specific Mass Change (mg/cm2)						
Time(h)	**FeCrAlSi**	**FeCrSi**	**25Cr FeCrAl**	**AFA 25Ni**	**AFA 20Ni**	**AFA 12Ni**	**Pure Ni**
0	0.00	0.00	0.00	0.00	0.00	0.00	0.00
50	0.56	1.08	0.68	1.52	2.89	2.64	0.20
100	1.41	1.23	1.80	2.37	4.58	-0.37	0.37
150	2.04	-0.30	2.28	3.05	5.58	0.18	0.61
200	2.01	-0.37	2.51	3.66	2.56	-2.97	1.01
250	2.51	-1.10	3.96	4.38	-17.31	-2.02	0.81
300	3.18	-1.63	3.69	4.90	-26.44	-10.63	1.03
350	3.14	-2.02	2.47	6.23	-27.72	-14.82	1.26
400	3.31	-3.16	0.50	6.73	-30.25	-20.60	1.11
450	3.24	-4.62	0.19	7.29	-34.14	-21.61	1.62
500	3.49	-6.64	-0.24	7.87	-38.80	-26.10	1.80
550	3.47	-8.53	-4.40	7.69	-41.12	-27.97	1.95
600	4.32	-8.57	-5.67	8.67	-41.35	-28.77	2.96
650	4.02	-7.89	-6.97	6.79	-44.01	-35.87	2.76
700	3.99	-9.01	-7.99				
750	3.80	-9.82	-7.16				
800	3.26	-12.32	-7.54				
850	3.87	-11.74	-7.52				
900	4.42	-11.12	-6.28				
950	4.65	-10.86					
1000	5.32	-10.08					

APPENDIX B: PREPARATION OF TEST SAMPLE ALLOYS

Description from Oak Ridge National Laboratory.

"Commercial 316L, 310S, and FeCrAlY alloys were procured in sheet form, 446 in round bar form, and the pure Ni and 201 in plate form. The three developmental AFA alloys were obtained in solutionized plate form from hot-rolled and machined ~15 kg vacuum induction melted ingots (alloy process details are provided in reference Brady et al. (2014)). The model FeCrAlSi, FeCrSi, and Fe25CrAl alloys were vacuum arc cast in small, laboratory scale 2.5 cm x 2.5 cm x 10 cm ingots, solutionized at 1200°C for 1 h in Ar-4H_2 gas, and then hot rolled at 1100°C to 50% reduction using 5-10% reduction per rolling pass. Test samples 20 x 10 mm x 0.75 to 1.2 mm for lab furnace evaluation and 2.5cm x 12.5cm x 0.75 to 1.2 mm with a 4 mm diameter hole for in-situ cookstove evaluation were electro-discharged machine (EDM) cut. For the thin sheet 316L, 310S, and FeCrAlY samples, the as-processed surface finish was retained for corrosion testing. For all of the other alloy product forms, the EDM-cut surface finish of the test sample faces was polished to 600 grit finish by standard metallographic techniques in water using SiC grinding papers" [23].